Coastal Engineering 80 (2013) 16–34

Contents lists available at SciVerse ScienceDirect

Coastal Engineering

journal homepage: www.elsevier.com/locate/coastaleng

A coupled model of submerged vegetation under oscillatory flow using Navier–Stokes equations

Maria Maza, Javier L. Lara *, Inigo J. Losada

Environmental Hydraulics Institute "IH Cantabria", Universidad de Cantabria, C/Isabel Torres no. 15 Parque Científico y Tecnológico de Cantabria 39011 Santander, Spain

ARTICLE INFO

Article history:
Received 12 February 2013
Received in revised form 25 April 2013
Accepted 29 April 2013
Available online xxxx

Keywords:
Vegetation
Wave dissipation
RANS model
Drag coefficient

ABSTRACT

This work presents a new model for wave and submerged vegetation which couples the flow motion with the plant deformation. The IH-2VOF model is extended to solve the Reynolds Average Navier–Stokes equations including the presence of a vegetation field by means of a drag force. Turbulence is modeled using a k–ε equation which takes into account the effect of vegetation by an approximation of dispersive fluxes using the drag force produce by the plant. The plant motion is solved accounting for inertia, damping, restoring, gravitational, Froude–Krylov and hydrodynamic mass forces. The resulting model is validated with small and large-scale experiments with a high degree of accuracy for both no swaying and swaying plants. Two new formulations of the drag coefficient are provided extending the range of applicability of existing formulae to lower Reynolds number.

1. Introduction

Vegetated coastal habitats, including seagrasses such as *Posidonia* and macroalgae such as Kelp, have received much attention in recent years for its role in providing several functions contributing to coastal protection. Among other factors their canopies contribute to dampen wave height and velocities (Fonseca and Cahalan, 1992; Koch, 2009; Mendez and Losada, 2004), reducing flow and turbulence (Nepf and Vivoni, 2000) and thereby promoting sedimentation and limiting sediment resuspension within the vegetation beds (Gacia and Duarte, 2001; Terrados and Duarte, 2000).

Researchers working on wave interaction with vegetation fields have recognized the complexity of the processes involved, especially due to the coupling between the waves and vegetation motion. Besides the fact that only through the integration of field work, physical experiments and theoretical/numerical models a detailed knowledge of said processes will be achieved, it has to be said that some progress has been achieved so far considering the different approaches.

Few examples of detailed field studies considering wave attenuation are present in the literature (Bradley and Houser, 2009; Elwany et al., 1995; Lowe et al., 2007).

Although this approach is the best suited to improve our understanding of the relevant processes, unfortunately, the ample range of species and hydrodynamic conditions considered and the technical complexity of the work do not guarantee, so far, the generalization of the results.

A second more extended approach has been the performance of small and large-scale experiments in wave flumes and basins under a controlled environment. Most of the laboratory experiments have been devoted to show that wave damping is strongly affected by different submerged aquatic species mostly represented by mimics selected to simulated real vegetation properties such as buoyancy and stiffness (Dubi and Torum, 1995) or even considering rigid artificial units (Lowe et al., 2005).

At a larger scale, Stratigaki et al. (2011), characterized wave attenuation produced by *Posidonia oceanica* using artificial flexible mimics. Some additional results on these experiments have been recently published in Koftis et al. (2013).

Only recently, a limited number of experiments with real vegetation have been presented in the literature (Bouma et al., 2013; Bridges et al., 2011; Maza et al., 2013). Although the existing experimental studies provide a good sensitivity analysis to different parameters involved in the wave interaction with wave vegetation, conclusions are restricted to inherent limitations associated to physical modeling.

Together with the main goal of improving our understanding of the relevant hydrodynamic processes, laboratory work has been the main source of validation for both theoretical and numerical models.

Early pioneering works provided the basis for the conceptual models of wave damping by submerged vegetation (Dalrymple et al., 1984; Dubi and Torum, 1997; Kobayashi et al., 1993; Mendez et al., 1999). This work has been later extended to consider random breaking and nonbreaking waves, Mendez and Losada (2004) or wave and current interaction with vegetation, Ota et al. (2004).

In order to overcome most of the limitations associated to the initial models two lines of research have been followed over the last years. For those interested in the effects originated by submerged vegetation fields on waves, currents and associated sediment transport, the approach has been performed introducing expressions for

* Corresponding author. Tel.: +34 942 20 16 16; fax: +34 942 20 18 60.
E-mail address: jav.lopez@unican.es (J.L. Lara).

0378-3839/$ – see front matter © 2013 Published by Elsevier B.V.
http://dx.doi.org/10.1016/j.coastaleng.2013.04.009

vegetation drag as a function of characteristics such as shoot density and canopy width based on previous approaches or empirical formulations derived from physical modeling into phase averaged models. Some examples are the full spectrum model SWAN (Suzuki et al., 2011), including the damping model by Mendez and Losada (2004) or Chen et al. (2007) considering the effects of seagrass bed geometry on wave attenuation and suspended sediment transport using a modified Nearshore Community Model (NearCoM).

In order to solve the near field or the kinematics and dynamics within the vegetation field several researchers have used phase resolving models with vegetation damping such as Boussinesq equation based models (Augustin et al., 2009). Furthermore, several advances in the analysis of airflow interaction with terrestrial plants (DuPont et al., 2010) using full Navier–Stokes equations, have opened the possibility to address the complex turbulent interaction between waves and submerged vegetation in the marine environment.

It has to be said that some early works exist in this context. Two-dimensional applications using Navier–Stokes equations have been already presented by Ikeda et al. (2001) and Li and Yan (2007). However, several aspects in their models are still undefined. Most of them are related to the correct definition of the horizontal and vertical velocities associated to the oscillatory flow, the treatment/lack of turbulence or of the coupled motion of fluid and plants as well as the definition of the drag force exerted by the flow on the individual plants.

During the last years much progressed has been achieved in the field in wave modeling based on RANS equations. Losada et al. (2008), Lara et al. (2008), Guanche et al. (2009), Torres-Freyermuth et al. (2007) or Lara et al. (2011) are a few examples of the capabilities of RANS equations combined with a Volume of Fluid technique that is able to deal with the modeling of wave interaction with different complex structures or surf zone processes.

Based on this work, the purpose of this paper is to provide a new numerical coupled model able to improve the existing models by introducing a higher degree of complexity in simulating the processes governing the interaction between waves and vegetation. Based on an existing Reynolds Average Navier–Stokes (RANS) equation model (IH-2VOF, Lara et al., 2008; Losada et al., 2008), the governing equations are extended to include the presence of a vegetation field by considering an additional friction, inducing a loss of momentum represented by a drag force. The restoring force is approximated by including the displacement at the top of a cantilever beam using the flow velocities. Besides, turbulence is modeled using a k–ε model which takes into account the effect of vegetation by an approximation of dispersive fluxes using the drag force produce by the plant after Hiraoka and Ohashi (2006). Comparisons between numerical and experimental results for small and large scale no swaying and swaying vegetation show a very high degree of agreement.

2. Equations and numerical model description

In this work, an extended version of the Navier–Stokes (NS) based model IH-2VOF is developed by introducing a coupled system of equations considering both the wave and plant motion. IH-2VOF (Lara et al., 2011; Losada et al., 2008) solves wave flow for hybrid two dimensional domains in a coupled NS-type equation system, in this case, at the clear-fluid region (outside the vegetation field) and inside the vegetation field. The movement of the free surface is tracked by the Volume of Fluid (VOF) method. This model based on the Reynolds Average Navier–Stokes (RANS) equations has been successfully applied in previous work for the study of wave–structure interaction and wave breaking on beaches. In particular, Torres-Freyermuth et al. (2007) employed the IH-2VOF model to investigate the near shore processes associated with random wave breaking on a gently sloping natural beach. Further they studied long wave transformation in beaches using a high spatial resolution laboratory dataset (Torres-Freyermuth et al., 2009) and Lara et al. (2011) and Ruju et al. (2012) studied long waves induced by transient wave group on a beach. About validation in flow-structure interaction Losada et al. (2008), Lara et al. (2008) and Guanche et al. (2009) show the satisfactory results obtained with this model.

At the clear-fluid region the 2DV RANS equations are considered. The flow inside the vegetation field is modeled considering an additional friction inducing a loss of momentum which is represented by a drag force, similar to Mendez et al. (1999):

$$\overline{F}_{D,i} = \frac{1}{2}\cdot C_D \cdot a \cdot N \cdot \overline{u}_{rel,i} \cdot \left|\overline{u}_{rel,i}\right| \tag{1}$$

where ρ is the flow density, a is the width of the vegetation element perpendicular to the flow direction, C_D is the drag coefficient, N is the number of plants per unit area and $\overline{u}_{rel}$ is the relative velocity defined as the difference between the plant and flow velocities. Sub-index i represents the components of the velocity and force vectors. Therefore the RANS equations inside the vegetation field are formulated by introducing this force in the momentum balance equation:

$$\frac{\partial \overline{u}_i}{\partial x_i} = 0 \tag{2}$$

$$\frac{\partial u_i}{\partial t} + \overline{u}_j \frac{\partial u_i}{\partial x_j} = -\frac{1}{\rho}\frac{\partial p}{\partial x_i} + g_i + \frac{1}{\rho}\frac{\partial \overline{\tau_{ij}}}{\partial x_j} - \frac{\partial \overline{\left(u'_i u'_j\right)}}{\partial x_j} - \overline{F}_{D,i} \tag{3}$$

where $\overline{u}$ is the mean flow velocity, t is the time, $\overline{p}$ is the mean pressure, x is the spatial coordinate, u' is the turbulent flow velocity and $\overline{\tau_{ij}} = 2\mu\overline{\sigma_{ij}}$ is the mean viscous tensor, being μ the molecular viscosity and $\overline{\sigma_{ij}} = \frac{1}{2}\left(\frac{\partial \overline{u_i}}{\partial x_j} + \frac{\partial \overline{u_j}}{\partial x_i}\right)$ the mean flow deformation rate. The term $\overline{\left(u'_i u'_j\right)}$ represents the Reynolds stresses, which take into account the turbulent flow.

In order to close Eq. (1), the plant velocity is modeled to calculate the relative velocity, $\overline{u}_{rel}$. A vegetation mechanical model, following the Morison equation and based on the damped oscillatory movement equation (Ikeda et al., 2001; Mendez et al., 1999) is formulated accordingly. The governing equation of the plant motion is given by:

$$m_0 \cdot \frac{\partial^2 \xi_i}{\partial t^2} + C \cdot \frac{\partial \xi_i}{\partial t} + \left(E \cdot I \cdot \frac{\partial^4 \xi_i}{\partial z^4}\right) = \\ = \frac{1}{2}\cdot\rho\cdot C_D \cdot a \cdot \left(\overline{u} - \frac{\partial \xi_i}{\partial t}\right)\cdot\left|\overline{u} - \partial\frac{\xi_i}{\partial t}\right| + \left(\rho_p - \rho\right)\cdot g \cdot V_p \cdot \frac{\partial \xi_i}{\partial z} + \rho \cdot V_p \cdot \frac{\partial \overline{u}}{\partial t} + \rho \cdot C_m \cdot V_p \cdot \left(\frac{\partial \overline{u}}{\partial t} - \frac{\partial^2 \xi_i}{\partial t^2}\right) \tag{4}$$

where $m_0 = (\rho_p + \rho \cdot C_m) \cdot V_p$, ρ_p is the vegetation density, C_m is the added mass coefficient, V_p is the volume of the plant per unit area, ξ_i is the plant displacement, C is the damping coefficient, E is the Young's modulus and I is the inertia moment of the cross section of the plant. The first and second terms on the left-hand side are the inertia and damping forces and the last term correspond to the restoring force. The terms on the right-hand side are the drag, gravitational, Froude–Krylov and hydrodynamic mass forces, respectively. Eq. (4) is a simplified model which considers a linear deformation of the plant in order to solve its oscillatory motion by vertically integrating over the plant length as proposed by Dupont et al. (2010). This assumption allows obtaining the plant deformation along its length as a function of the tip deformation angle as a first approximation. As long as the vegetation deformation is not very large this approximation gives good results and the computational cost used to solve the plant motion is very low. However, for very flexible vegetation this approach allows obtaining the maximum plant displacements but not the deformation along the vegetation length. When this

Table 1
Values of empirical constant of k–ε turbulence model.

κ	0.4
σ_k	1.0
σ_ε	1.3
C_μ	0.09
$C_{\varepsilon 1}$	1.44
$C_{\varepsilon 2}$	1.92
C_{kp}	1
$C_{\varepsilon p}$	3.5
C_D	Calibration

deformation is desired a model based on large deformations must be taken into account (Maza, 2012).

The integration of the plant motion is solved considering a linear deformation of the plant and the relative velocity is obtained as:

$$\overline{u}_{rel,i} = \overline{u}_i - \frac{\partial \xi_i}{\partial t}. \tag{5}$$

The relative velocity presented in Eq. (5) is also present in the first term of the right hand side of Eq. (4) which represents the drag force contribution.

This model differs from the one presented by Mendez et al. (1999) which is based on linear wave theory on a flat bottom whereas the presented model solves Navier–Stokes equations for variable depth. Furthermore, the proposed model not only allows modeling cases with submerged but also emerged vegetation. The model proposed in Ikeda et al. (2001) also differs from the one presented here. Although the same equations are used, the solving procedure is different. Ikeda et al. (2001) solve the restoring force considering an exponential velocity profile which determines the displacement values. In this model, the restoring force is approximated considering the displacement at the top of a cantilever beam under uniform loading using the flow velocities as the forcing loads. Ikeda et al. (2001) prescribe the plant deformation following an exponential deformation, therefore limiting the solutions.

Moreover, unlike in previous models (Ikeda et al., 2001; Mendez et al., 1999), turbulence is considered. Turbulence is modeled using a k–ε equation for the turbulent kinetic energy (k), and the turbulent dissipation rate (ε) which takes into account the effect of vegetation. The influence of turbulence fluctuations on the mean flow field is represented by the Reynolds stresses. The governing equations for k–ε are derived from the Navier–Stokes equations, and higher order correlations of turbulence fluctuations in k and ε equations are replaced by closure conditions. The effect of the vegetation field is considered by two additional terms, one in the turbulent kinetic budget, k_w, and the other one in the turbulent dissipation rate, ε_w. These terms take into account the production of turbulent kinetic energy and the energy dissipation produced inside the vegetation field by an approximation of dispersive fluxes using the drag force produce by the plant. The equations are based on the turbulence model presented by Hiraoka and Ohashi (2006), but closure terms are modified in order to consider the relative velocity developed only inside the vegetation meadow. Terms related to turbulent production and dissipations are considered only using the shear stress tensor according to the ensemble velocity. Therefore, the new k–ε model is presented as:

$$\rho\frac{\partial k}{\partial t} + \rho\overline{u}_j\frac{\partial k}{\partial x_j} = \frac{\partial}{\partial x_j}\left[\left(\frac{\mu_t}{\sigma_k}+\mu\right)\frac{\partial k}{\partial x_j}\right] + \tau_{ij}\frac{\partial \overline{u}_i}{\partial x_j} - \rho\varepsilon + \underbrace{+\rho C_{kp}C_D aN\sqrt{\overline{u}_{rel,j}\overline{u}_{rel,j}}k}_{k_w} \tag{6}$$

$$\rho\frac{\partial \varepsilon}{\partial t} + \rho\overline{u}_j\frac{\partial \varepsilon}{\partial x_j} = \frac{\partial}{\partial x_j}\left[\left(\frac{\mu_t}{\sigma_\varepsilon}+\mu\right)\frac{\partial \varepsilon}{\partial x_j}\right] + C_{\varepsilon 1}\frac{\varepsilon}{k}\tau_{ij}\frac{\partial \overline{u}_i}{\partial x_j} - C_{\varepsilon 2}\rho\frac{\varepsilon^2}{k} + \underbrace{+\rho C_{\varepsilon p}C_D aN\sqrt{\overline{u}_{rel,j}\overline{u}_{rel,j}}\varepsilon}_{\varepsilon_w}. \tag{7}$$

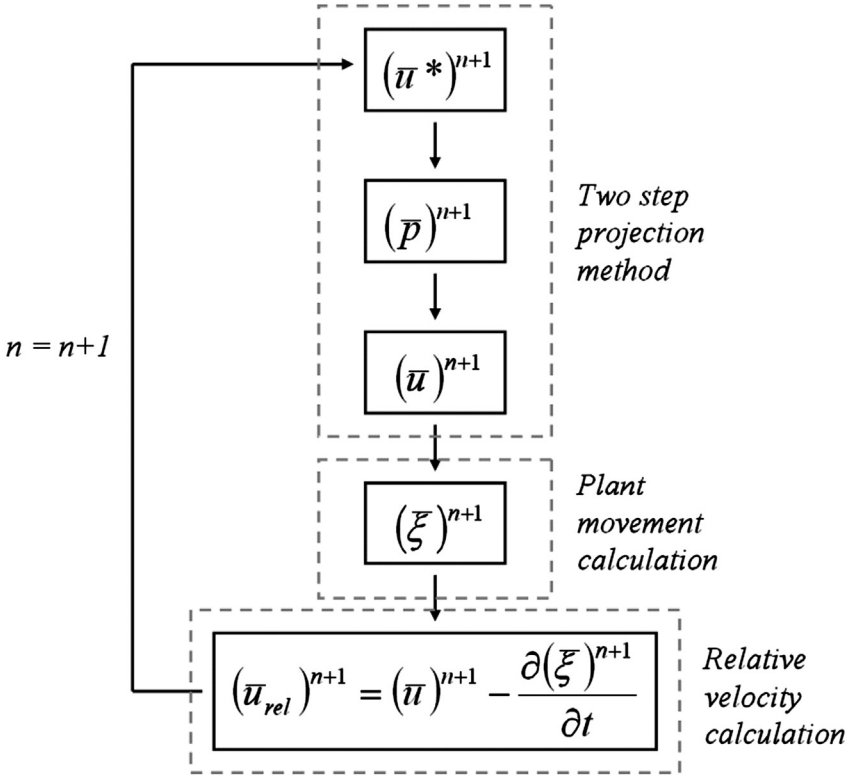

Fig. 1. Flowchart of the solving procedure.

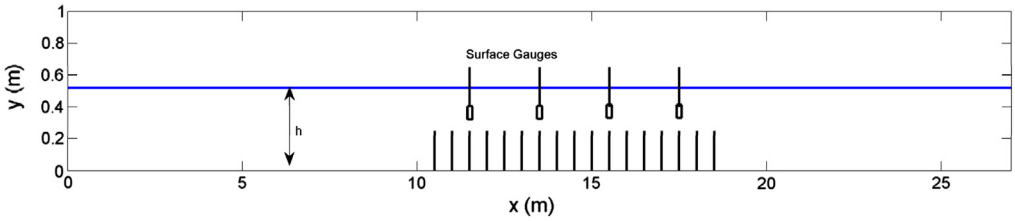

Fig. 2. Asano et al. (1988) experimental set-up. Vegetation field is represented by vertical solid black lines and the positions of free surface gauges are displayed.

In the equations above μ_t is the eddy viscosity, μ is the dynamic viscosity and σ_k is a closure coefficient. Values given by Hiraoka and Ohashi (2006) for the empirical constants C_{kp} and $C_{\varepsilon p}$ are used (see Table 1). The drag coefficient, C_D, is the same coefficient used in the momentum equation.

Besides the equations presented above, there are two additional relations needed to make use of the k–ε model. The first introduces the Boussinesq approximation which assumes that Reynolds stresses (τ_{ij}) are directly proportional to the mean strain-rate tensor ($\overline{S}_{ij}$).The proportionality constant is the eddy or turbulent viscosity, μ_t,

$$\rho\left(\overline{u'_i u'_j}\right) = 2\mu_t \overline{S}_{ij} - \frac{2}{3}\rho k \delta_{ij} \tag{8}$$

where the last term in the previous equation is introduced for consistency reasons. Having defined the Reynolds stresses, there is only the need to define the eddy viscosity in order to link the k–ε model with the momentum conservation equations. By dimensional considerations the eddy viscosity is defined as,

$$\mu_t = \rho C_\mu \frac{k^2}{\varepsilon} \tag{9}$$

where C_μ is an empirical constant (Table 1).

IH-2VOF uses a finite difference scheme to discretize the equations. A forward time difference and a combined central difference and upwind schemes are considered for the time and spatial derivations,

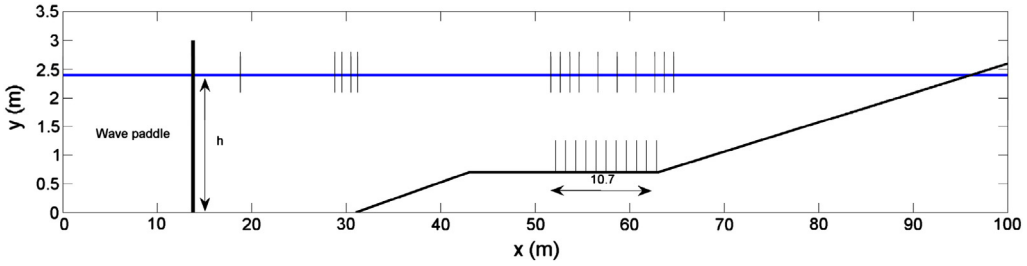

Fig. 3. Stratigaki et al. (2011) experimental set-up. Vegetation field is represented by vertical solid lines and the positions of free surface gauges are displayed.

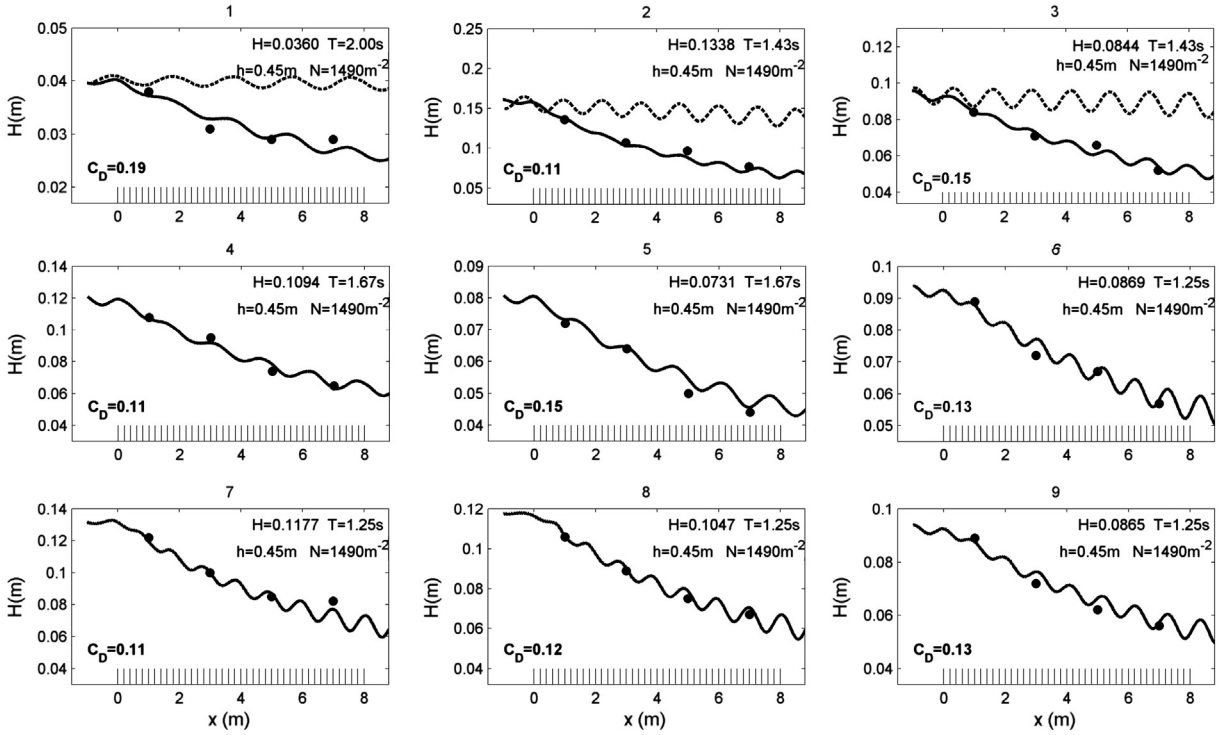

Fig. 4. Numerical results(solid line) and Asano et al. (1988) laboratory data(black dots) of wave evolution along the meadow for experiments 1-9. Wave evolution without vegetation (dashed line) is presented in images 1-3.

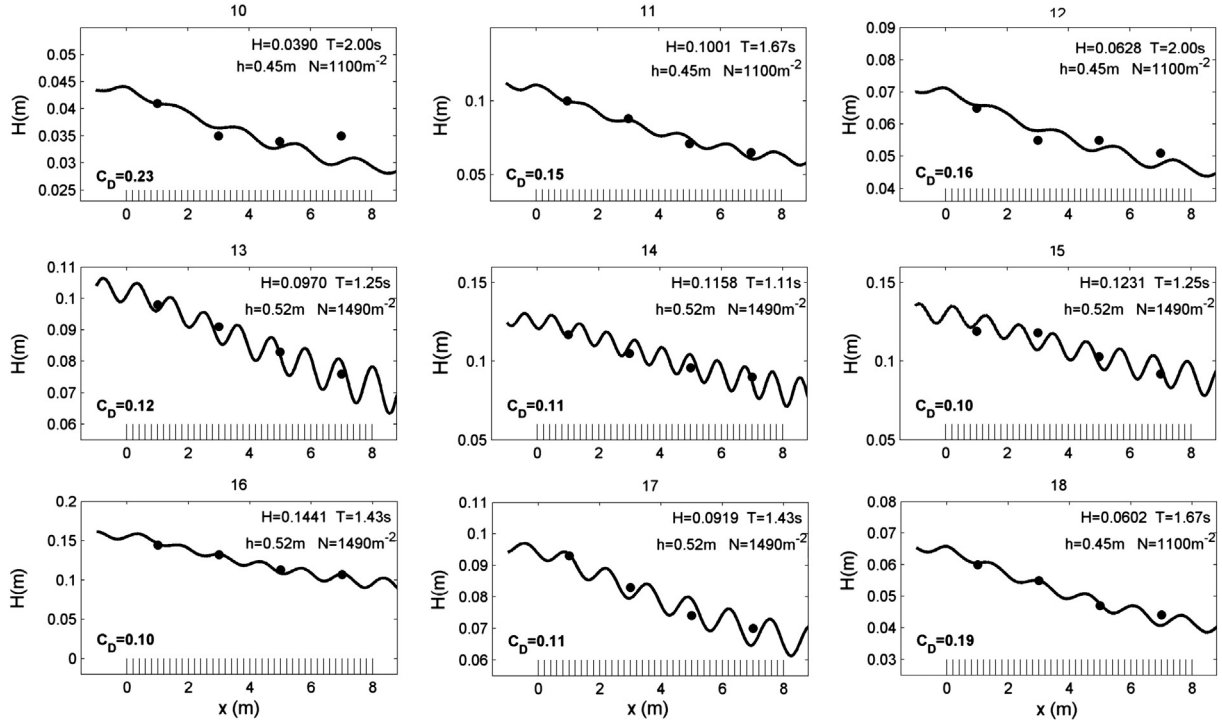

Fig. 5. Numerical results (solid line) and Asano et al. (1988) laboratory data (black dots) of wave evolution along the meadow for experiments 10–18.

respectively. A two-step projection method is used in the resolution of the equations. The turbulence model is solved based on an explicit finite difference scheme.

Wave conditions are introduced in the model imposing a velocity field and a free surface time evolution at one side of the numerical domain. Active wave absorption, Torres-Freyermuth et al. (2009), is also considered, not only at the rear end of the numerical flume to allow waves leaving the domain but also at the wave generating boundary, so that they do not interfere with the generated waves.

The solving procedure consists of coupling both the fluid and the plant motion. Flow velocities are used to calculate the induced plant motion using Eq. (4) following an explicit time marching scheme using forward differencing. Once the plant motion is solved it is used to obtain the relative velocity, Eq. (5). This relative velocity is used to update

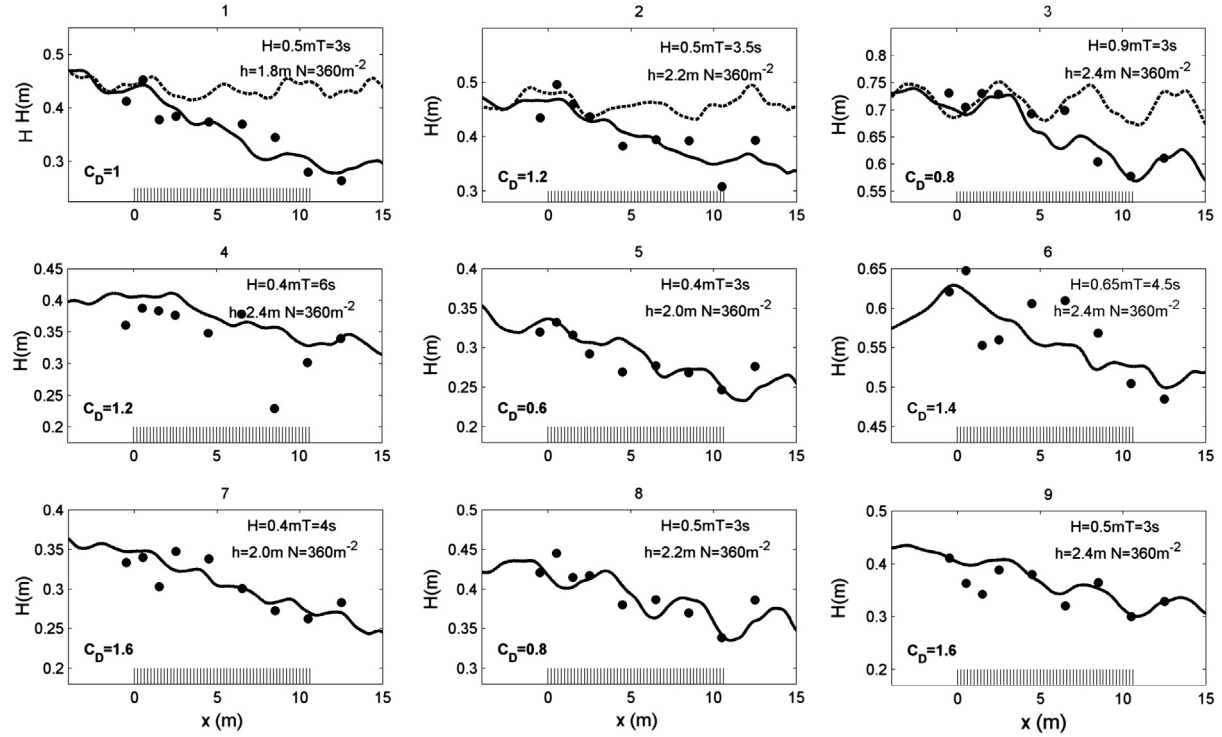

Fig. 6. Numerical results (solid line) and Stratigaki et al. (2011) laboratory data (black dots) of wave evolution along the meadow for experiments 1–9. Wave evolution without vegetation (dashed line) is presented in images 1-3.

the velocity used in the two step projection method at the next time step. In this way, the relative velocities calculated at a given time step allow obtaining the plant motion which will be used to evaluate the relative velocity at the next time step. Fig. 1 shows a flowchart with the solving procedure.

3. Numerical model validation

Although an extensive validation of IH-2VOF model has been carried out for other flow conditions, validation for this new implementation is needed. In this work, the coupled motion of flow and vegetation is validated using experimental studies available in the literature. The validation is carried out in two steps. First, a simplified approach to the problem is considered by modeling the flow interaction with no swaying vegetation, see for instance Lowe et al. (2005). Secondly, the coupled movement between flow and vegetation is considered.

In the first case, the problem is simplified because the relative velocity is directly the flow velocity. The introduction of a new equation to describe the motion of the plants is not needed. Therefore, with no swaying elements the vegetation effect is reduced to evaluating the drag force presented in Eq. (1) obtained as a function of the flow velocity (Lowe et al., 2005; Mendez et al., 1999). In order to validate this approach numerical results are compared with experimental data from flume experiments developed by Asano et al. (1988). These experiments have been previously used to validate similar models, Mendez et al. (1999). A second set of experiments with flexible vegetation is also considered to validate this approach. These experiments are the ones presented in Stratigaki et al. (2011).

Once this validation is completed, the second approach, which considers the coupled movement between the flow and the vegetation, is validated using Stratigaki et al. (2011) experimental data.

In order to carry out both validations the set of coefficients defined in the model must be specified. The k–ε model coefficients are kept constant. Considering no swaying vegetation the only parameter to be set is the drag coefficient, C_D, which will be used as the calibration coefficient. Considering the coupled movement requires the added mass and the damping coefficients to be determined together with the drag coefficient which will be again the calibration coefficient. The values of these coefficients will be specified further on.

Table 2
Drag coefficient and Reynolds number values for 18 cases of Asano et al. (1988) and Stratigaki et al. (2011) experiments.

Case	Asano et al. (1988)		Stratigaki et al. (2011)	
	Re	C_D	*Re*	C_D
1	4763	0.19	4697	1.6
2	12,367	0.11	5429	1.2
3	8520	0.15	4546	1.2
4	13,263	0.11	8455	0.8
5	9441	0.15	4700	0.6
6	9373	0.13	7058	1.4
7	11,642	0.11	4595	1.6
8	11,165	0.12	5230	0.8
9	9373	0.13	5542	1.2
10	10,469	0.10	4697	2.4
11	8461	0.11	5122	1.48
12	9981	0.10	5350	1.2
13	8652	0.12	6687	1
14	9429	0.11	5625	0.8
15	8075	0.16	6896	2
16	5164	0.23	7031	0.8
17	11,455	0.15	6896	2
18	7221	0.19	3758	0.68

3.1. A brief description of the numerical experiments used for validation

A brief description of the experiments to be numerically modeled is given in the following:

Asano et al. (1988)

Asano et al. (1988) experiments were carried out in a 27 m long, 0.5 m wide and 0.7 m high flume. Vegetation mimics were made with polypropylene strips with a specific gravity of 0.9. Each of the strips was 25 cm long, 5.2 cm wide and 0.03 mm thick. The artificial vegetation field had a length of 8 m and was disposed in the middle

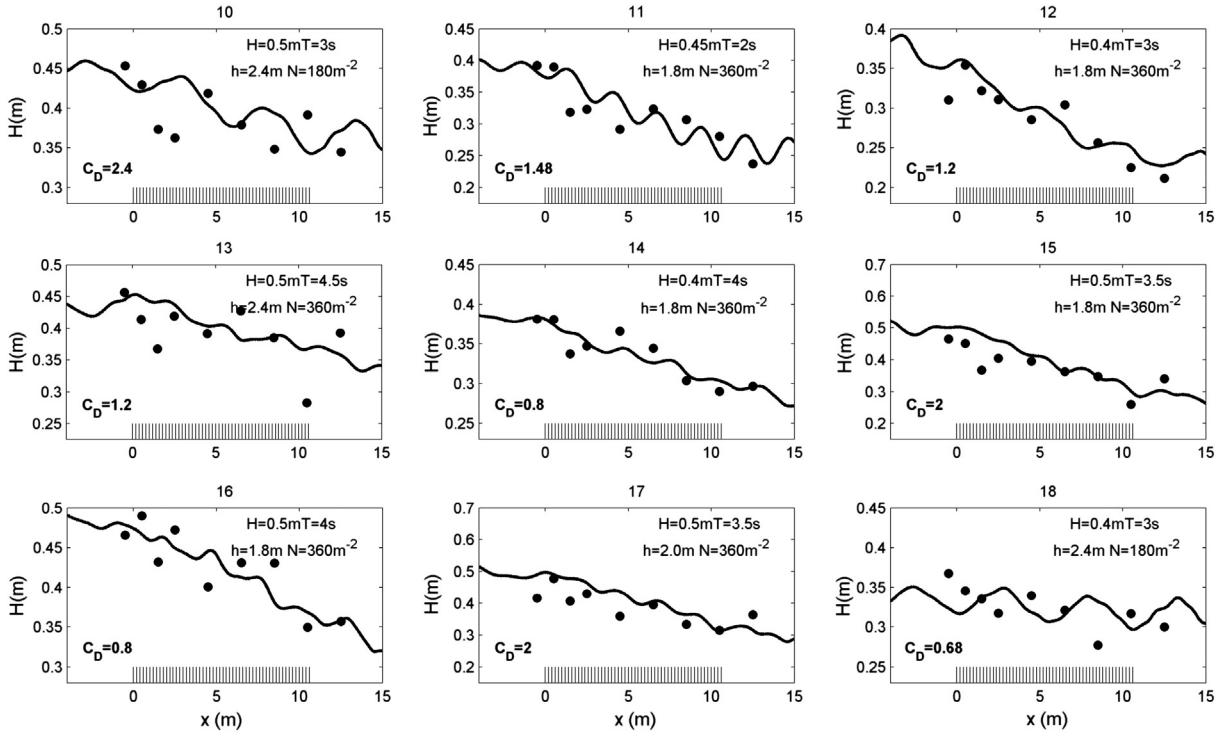

Fig. 7. Numerical results (solid line) and Stratigaki et al. (2011) laboratory data (black dots) of wave evolution along the meadow for experiments 10–18.

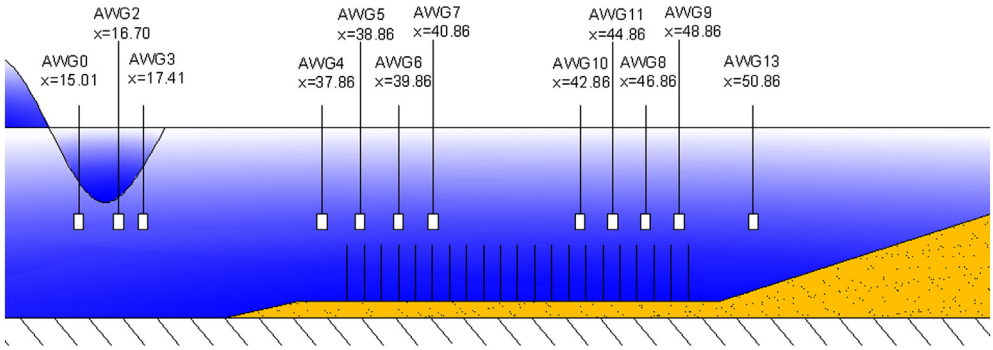

Fig. 8. Scheme of the free surface gauges location for Stratigaki et al. (2011) experiments.

of the flume width. For the entire test runs capacitance wave gauges were used to measure the free surface oscillations at four locations over the artificial vegetation field. The first one was located 1 m from the edge of the field and the distance between two adjacent gauges was 2 m, as it is shown in Fig. 2.

Two different seaweed densities, N, were tested. The sparse configuration had 0.110 strips/cm^2 whereas the dense configuration consisted of 0.149 strips/cm^2. Two different water depths (h), were evaluated, h = 45 and 52 cm. For the different combinations of N and h, except for the case of N = 0.110 strips/cm^2 and h = 52 cm different monochromatic waves were generated. Eight different wave frequencies were considered, f = 0.5, 0.6, 0.7, 0.8, 0.9, 1.0, 1.2 and 1.4 Hz. Six different wave heights were tested for the frequency of 0.8 Hz and two for the other cases. A total of sixty tests were carried out and for each one of them the values of the wave height in the different capacitance gauges were measured.

Stratigaki et al. (2011)

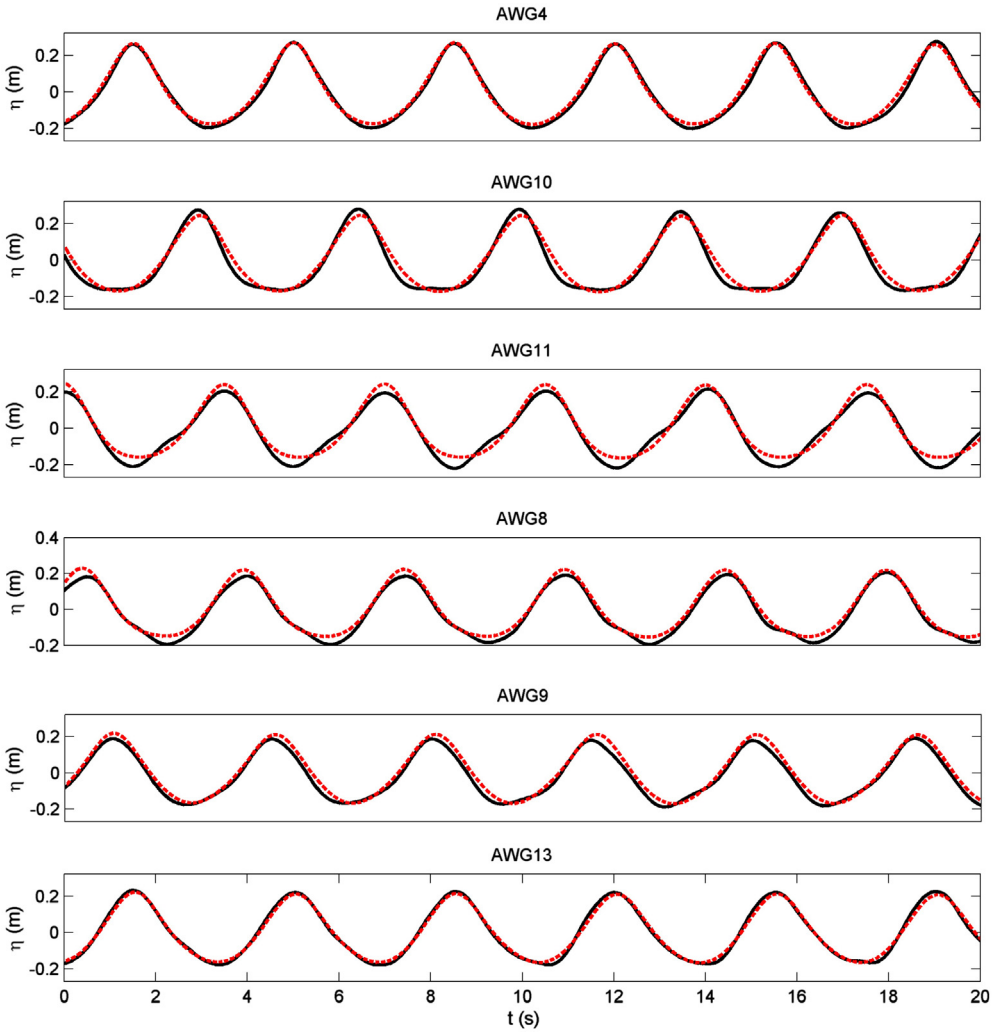

Fig. 9. Free surface time series for 1 gauge located before the meadow and 5 inside it. Laboratory data (black line) and numerical results (red dashed line) for the experiment with N = 180 m^{-2}, h = 2.4 m, H = 0.5 m and T = 3.5 s. (For interpretation of the references to color in this figure legend, the reader is referred to the web version of this article.)

These experiments were carried in the UPC flume in Barcelona. Flume dimensions were 100 m long, 3 m wide and 5 m deep. Due to these dimensions experiments were scaled. The flume bottom was covered by a sandy layer 0.7 m thick and at a distance equal to 17.21 m from wave paddle generation a 1/15 slope of 12 m was located. Behind this slope, a 20 m flat sandy beach was located and finally a beach of 37 m to dissipate wave energy. Over the flat sandy beach a 10.7 m long artificial vegetation field was placed. The beginning of this vegetation field was located at 38.36 m from the wave paddle.

Vegetation mimics were composed of four PVC strips, one pair 45 cm long and another pair of 27.5 cm length, all inserted in a stiff 10 cm long rod of the same material. PVC strips were 1 mm thick and 1 cm wide, with a Young's modulus equal to 2.9 GPa and a density equal to 700 kg/m^3.

Two densities were tested, 360 mimics/m^2 and 180 mimics/m^2. Free surface measurements were taken with fifteen resistive gauges, six before the meadow, seven over it and two after the field as shown in Fig. 3. Velocity was measured using eight ADVs (Acoustic Doppler Velocimeters) and four EMCMs (Electro Magnetic Current-meters) positioned at three different distances from the paddle, at 37.66, 40.36 and 46.36 m. EMCMs allowed measuring velocity inside the field.

Different wave conditions were tested. As the present study is focused on regular waves, a total of 54 runs are available for the validation. These runs were the results of the combination of different wave heights, periods, water depths and meadow densities. The tested wave conditions were the result of considering values of significant wave height between 0.4 and 0.5 m, wave periods between 2 and 6 s and water depths of 1.8, 2.0, 2.2 and 2.4 m.

3.2. Validation for no swaying vegetation

The no swaying vegetation approach considers the vegetation effect as a loss of energy modeled by a drag force. For this propose, different wave and vegetation conditions are simulated with the model IH-2VOF.

For modeling Asano et al. (1988) experiments a uniform grid size is chosen. In the horizontal direction the grid size is equal to 0.02 m and in the vertical equal to 0.005 m. In the case of Stratigaki et al. (2011) experiments, a large grid is used due to the experimental scale and a uniform grid system of variable grid size is used. The smallest discretization is used where the vegetation is located, having a grid size equal to 0.04 m in the horizontal direction and half of this value, 0.02 m, in the vertical one. The grid size has been selected on the basis of experience achieved in previous applications of the model.

To verify the simulated wave conditions the measurements of the first free surface gauges for both experiments are compared with the numerical results obtained at that position. Once the same wave conditions are obtained numerically all the variables involved in the problem are known except the drag coefficient. Therefore, this coefficient will be the calibration parameter of the model.

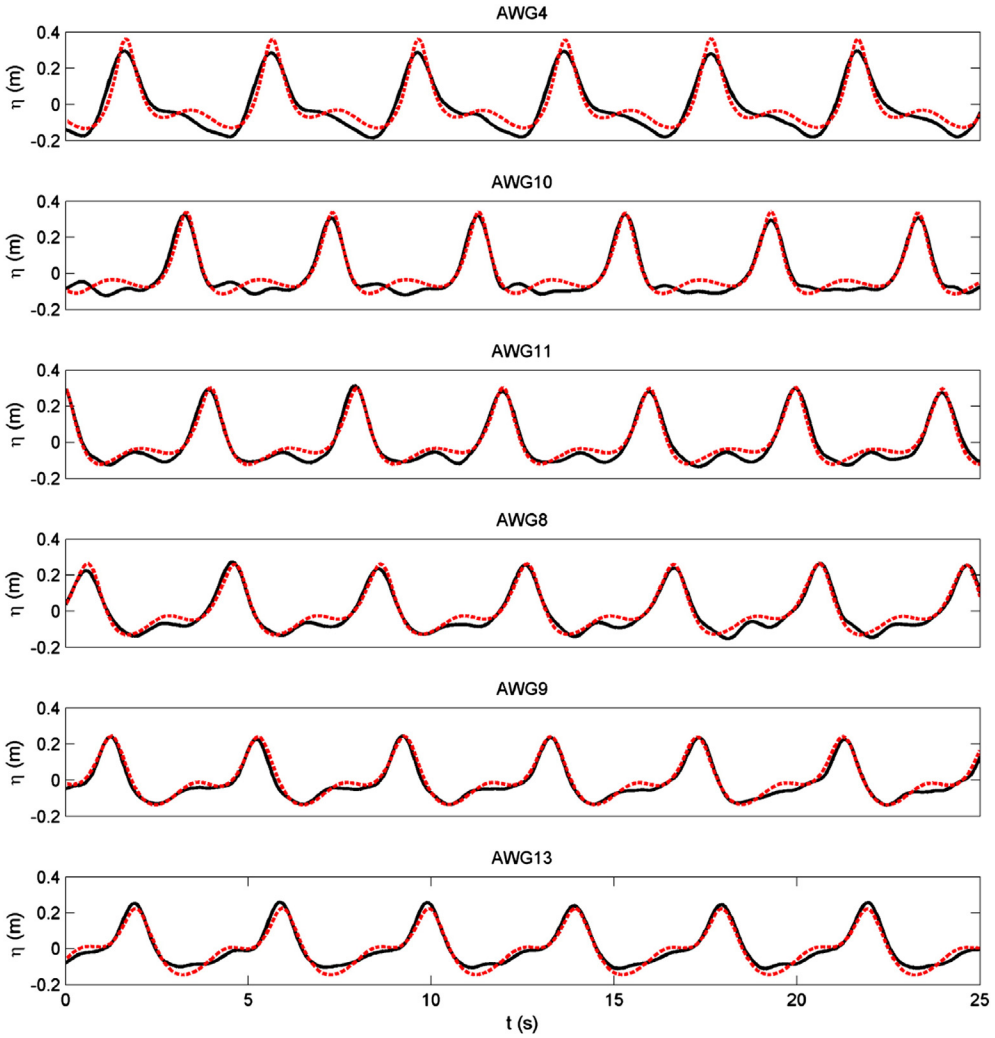

Fig. 10. Free surface time series for 1 gauge located before the meadow and 5 inside it. Laboratory data (black line) and numerical results (red dashed line) for the experiment with N = 360 m^{-2}, h = 1.8 m, H = 0.5 m and T = 4 s. (For interpretation of the references to color in this figure legend, the reader is referred to the web version of this article.)

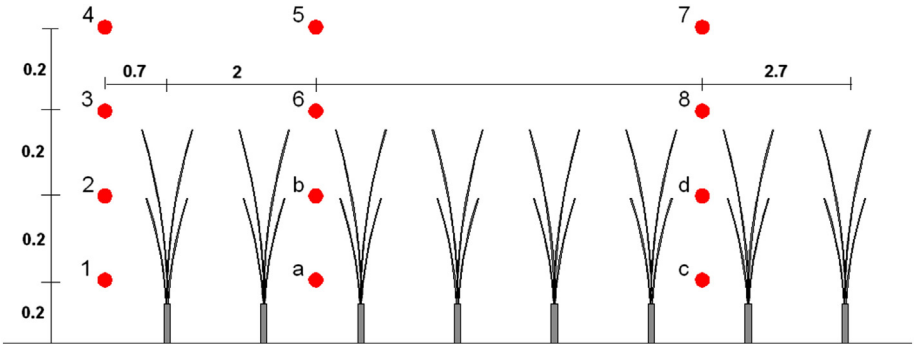

Fig. 11. ADVs (1–8) and EMCMs (a–d) locations for Stratigaki et al. (2011) experiments.

3.2.1. Wave height evolution

Sixty tests carried out by Asano et al. (1988) are simulated and the wave evolution over the plant meadow is compared. The results for eighteen of these tests are shown in Figs. 4 and 5. In each one of them the flow and vegetation conditions are displayed as well as the value of the drag coefficient used to fit the wave evolution along the field. As can be observed in the figure there is a good agreement in all cases. The model allows reproducing wave attenuation for different wave conditions, water depth and vegetation density. It is observed that wave attenuation is higher for larger relative depths (defined as the ratio between the vegetation height and the water depth) higher vegetation densities and larger Reynolds numbers (around 5000–7000) with wave height attenuations up to 60%. Small variations for the drag coefficient are shown with the largest values of the Reynolds number associated to the longer wave periods. In order to evaluate the real dissipation produced by the vegetation some runs are selected and simulated without considering vegetation. Only cases with relevant wave attenuation are chosen. Three of these simulations are shown in Fig. 4 in black dashed line. As can be seen the dissipation without vegetation is negligible whereas the simulations carried out with vegetation show a significant wave attenuation as the one measured in the experiments.

The experiments performed by Stratigaki et al. (2011) are also reproduced. In this case, the fifty four runs tested considering regular wave conditions are simulated. Eighteen of these runs are shown in Figs. 6 and 7. The numerical results fit the experimental measurements for different flow and vegetation conditions. Again, the drag coefficient used in each simulation is shown in each figure. This coefficient allows obtaining wave evolution along the field. This evolution leads to wave height attenuations up to 40% for cases with the largest

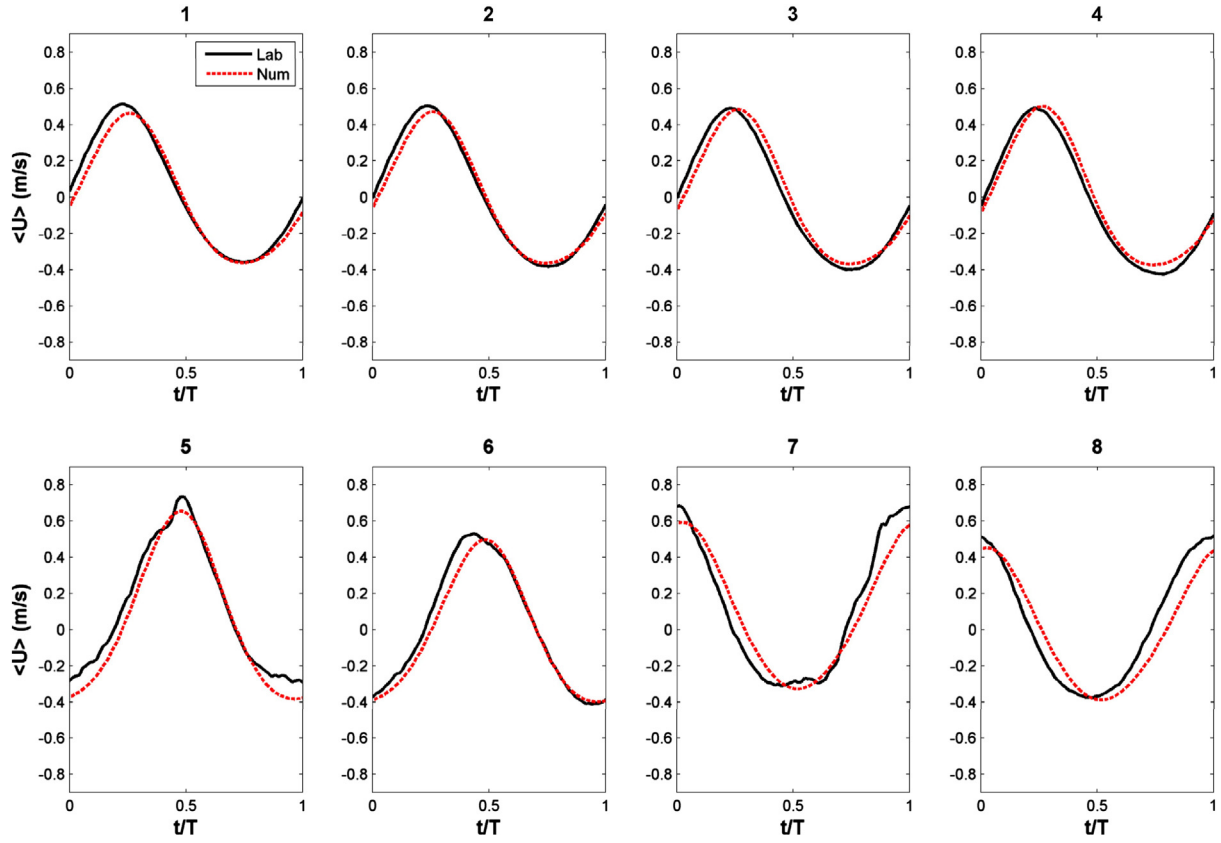

Fig. 12. Phase-averaged horizontal velocities, <U>, in front, 1–4, and above the meadow, 5–8 for the experiment with N = 180 m^{-2}, h = 2.4 m, H = 0.5 m and T = 3.5 s. Experimental data (black solid line) vs numerical results (red dashed line). (For interpretation of the references to color in this figure legend, the reader is referred to the web version of this article.)

vegetation density, the smallest water depth and large Reynolds numbers. Again three runs without vegetation are displayed in Fig. 6 showing negligible wave attenuation during wave propagation.

As a conclusion assuming no swaying stems and calibrating the C_D allows reproducing wave attenuation along the field using the convenient drag coefficient. The different complex processes produce in the interaction between flow and submerged vegetation are reproduced with a macroscopic approach based on a drag force.

From the different numerical experiments a set of drag coefficients has been found for Asano et al. (1988) and Stratigaki et al. (2011) experiments. The calculated values of the drag coefficient can be related with flow characteristics. Considering a Reynolds number, *Re*, defined as follows:

$$Re = a\frac{V_c}{\nu} \tag{10}$$

where a is the mimic width, V_c is the characteristic velocity, defined as the maximum value of the horizontal velocity at the top of the first mimic of the field and ν is the kinematic viscosity. This number has been used for authors such as Mendez et al. (1999) to account for flow characteristics. Table 2 shows the values for the drag coefficient for the 18 cases displayed in Figs. 4 and 5 for Asano et al. (1988) experiments, and in Figs. 6 and 7 for Stratigaki et al. (2011) experiments, and their associated Reynolds number.

As can be observed in the table, Reynolds numbers associated to the 18 tests of Asano et al. (1988) are higher than the values for Stratigaki et al. (2011). The opposite relationship between drag coefficient and Reynolds number is observed, with higher drag coefficients for Stratigaki et al. (2011).

Free surface data from Stratigaki et al. (2011) experiments are used in order to compare experimental and numerical time series. The location of the different gauges is shown in Fig. 8. Comparisons for two different cases are plotted in Figs. 9 and 10. Fig. 9 shows a case with the lowest vegetation density, N = 180 m^{-2}, and the deepest water depth, h = 2.4 m, with H = 0.5 m and T = 3.5 s. The numerical results reproduce with high accuracy the free surface measurements during the experiments, at both offshore (gauge AWG4), on the vegetation patch (gauges AWG10, 11, 8 and 9) and onshore (gauge AWG13). An additional case is shown in Fig. 10 for an N = 360 m^{-2} vegetation density case and a water depth of h = 1.8 m. The figure reveals larger wave deformation on the wave shape due to the higher influence of the vegetation meadow. Free surface attenuation and the nonlinearities produced by the interaction of the wave field with the vegetation meadow are well represented by the model as can be seen in the figure. The differences observed between laboratory and numerical results at the wave trough are due to unknown reflection patterns in the experiments at the rear end of the wave flume by the sandy beach, which is not simulated in the model.

3.2.2. Velocities inside and outside the meadow

The proposed approach is also validated using velocity measurements. The model IH-2VOF allows obtaining both, vertical and horizontal velocity components in the entire water column. Velocities predicted by the model are compared with measurements by Stratigaki et al. (2011).

Measurements inside, using EMCMs, and outside the meadow, using ADVs, were taken. The measurements are located at 37.66 m, 40.36 m and 46.36 m from the wave paddle which means at 0.7 m before the meadow, at 2 m from its beginning and at 2.7 m from its end. Fig. 11 shows a sketch of these locations. Numerical and experimental data

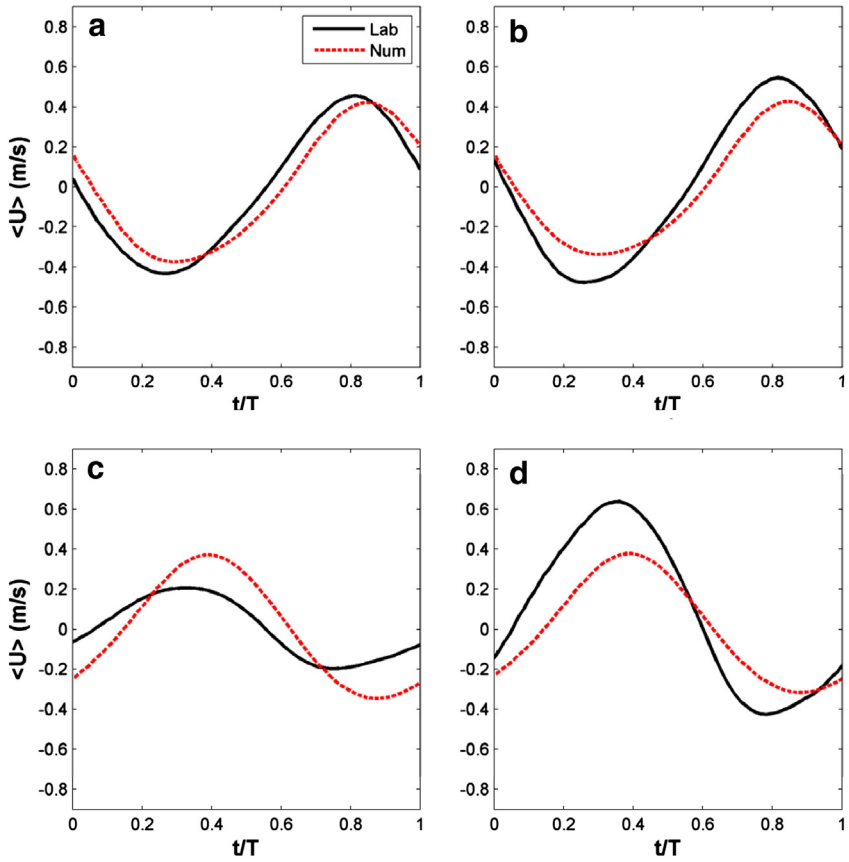

Fig. 13. Phase-averaged horizontal velocities, <U>, inside the meadow for the experiment with N = 180 m^{-2}, h = 2.4 m, H = 0.5 m and T = 3.5 s. Experimental data (black solid line) vs numerical results (red dashed line). (For interpretation of the references to color in this figure legend, the reader is referred to the web version of this article.)

are phase averaged over 20 waves for comparison. Figs. 12 and 13 show comparisons for horizontal velocity values, outside and inside the meadow respectively, and Figs. 14 and 15 vertical velocity values, for a test with H = 0.5 m, T = 3.5 s, h = 2.4 m and a vegetation density equal to 180 m^{-2}. In Figs. 12 and 14 the nonlinearities generated above the meadow are well captured by the numerical model as is shown in the comparisons at points 5, 6, 7 and 8. The measured velocities inside the meadow displayed in Fig. 13 show a good agreement in points *a* and *b* with small deviations in magnitude and a small phase shift. The results of point *c* and *d* show some discrepancies. Differences found in *c* and *d* can be due to a change in the sand bottom or local effects not captured by the model. Similar results are found in the velocity vertical components as presented in Fig. 15. The irregularities in laboratory measurements found in points *a*, *b* and *d* in this figure can be due to EMCM accuracy since very small values are registered.

Velocities are also validated by representing velocity profiles. Figs. 16 and 17 present minimum, mean and maximum velocity profiles for both, horizontal and vertical velocities for two different cases. Fig. 16 shows the results for a case with H = 0.5 m, T = 3.5 s, h = 2.4 m and N = 180 m^{-2}. This figure clearly indicates an increase in the horizontal velocity just above the meadow for both the numerical and experimental results. This is known as skimming flow and is the result of the strong discontinuity in the drag force between the area occupied by the meadow and the free flow over it. As can be observed the model is able to reproduce this phenomenon accurately. On the other hand, Fig. 17 displays the results for a case with H = 0.5 m, T = 4 s, h = 1.8 m and N = 360 m^{-2} in which the vegetation influence is stronger. In this case there is a larger velocity reduction inside the meadow and, again, the skimming flow is observed.

In general, a good agreement is found between laboratory and numerical data reproducing especially well the mean values, even for cases in which the vegetation influence is very important. Values recorded at point *c* are very small in comparison with the values measured at the rest of the points. The differences between the predicted and measured velocities at point *c* can be due to local effects, not considered in the numerical simulations, such as possible ripple formation during the experiments since the mimics were placed over a sandy bottom. This can be seen in the last plots of Figs. 16 and 17, where the point closest to the bottom presents a very small velocity value.

3.2.3. Drag coefficient values and fitting formulation

Authors, as Kobayashi et al. (1993) and Mendez et al. (1999), developed new empirical relationships for drag coefficient as a function of the Reynolds number, *Re*. Those formulas are a function of three parameters, α, β and γ, following the generic form:

$$C_D = \alpha + \left(\frac{\gamma}{Re}\right)^{\beta}. \tag{11}$$

Kobayashi et al. (1993) proposed values for these parameters based on the experimental data from Asano et al. (1988). Mendez et al. (1999) also proposed some values based on the same experiments using their own model considering both no swaying and swaying plants. Values in both papers are presented in Table 3.

As can be seen the values of Kobayashi et al. (1993) and Mendez et al. (1999) without plant swaying are almost identical whereas including plant swaying points to larger values of the drag coefficient.

In the calibration of the proposed model using Asano et al. (1988) and Stratigaki et al. (2011) experiments a set of drag coefficient values have been obtained. In order to relate these values with the empirical relationships described above the Reynolds number is obtained for each one of the runs. The calibrated drag coefficients obtained for Asano et al. (1988) experiments are represented in Fig. 18. The formulations proposed by Kobayashi et al. (1993) and Mendez et al. (1999),

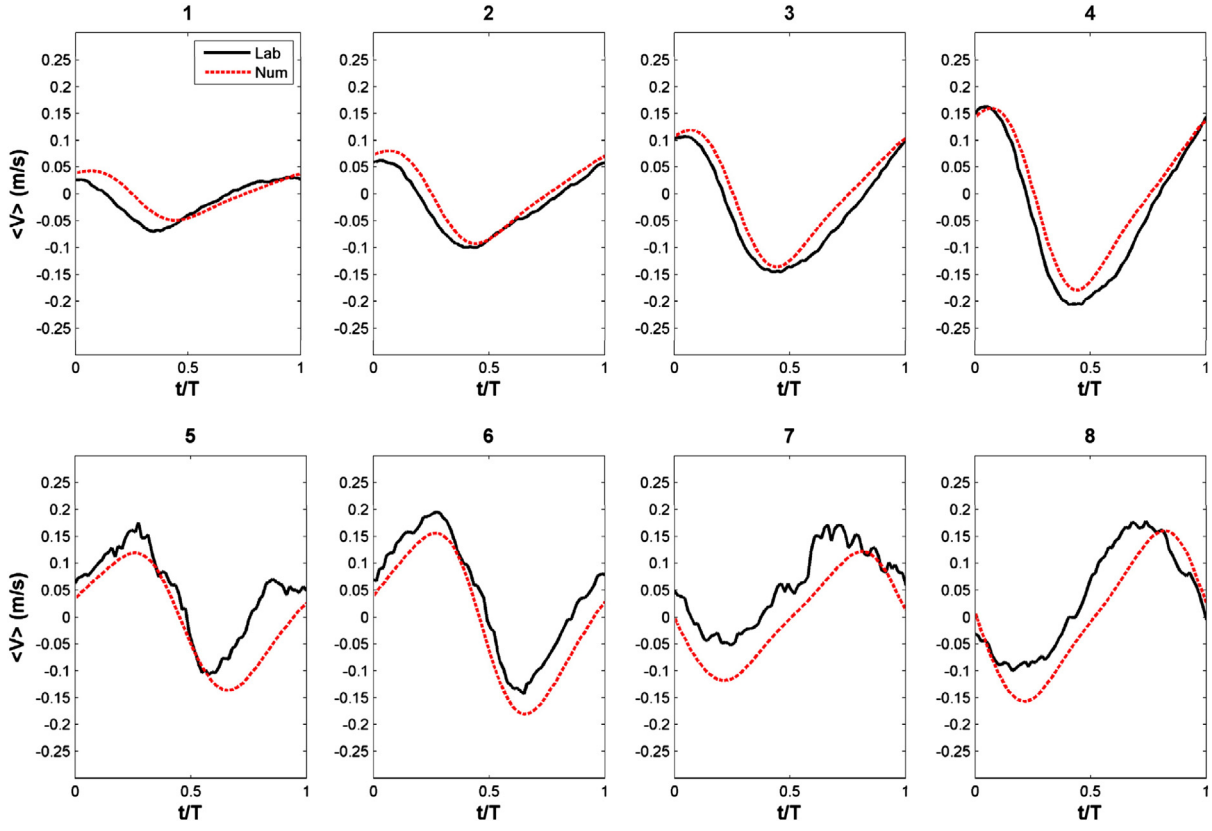

Fig. 14. Phase-averaged vertical velocities, <V>, in front, 1–4, and above the meadow, 5–8 for the experiment with N = 180 m^{-2}, h = 2.4 m, H = 0.5 m and T = 3.5 s. Experimental data (black solid line) vs numerical results (red dashed line). (For interpretation of the references to color in this figure legend, the reader is referred to the web version of this article.)

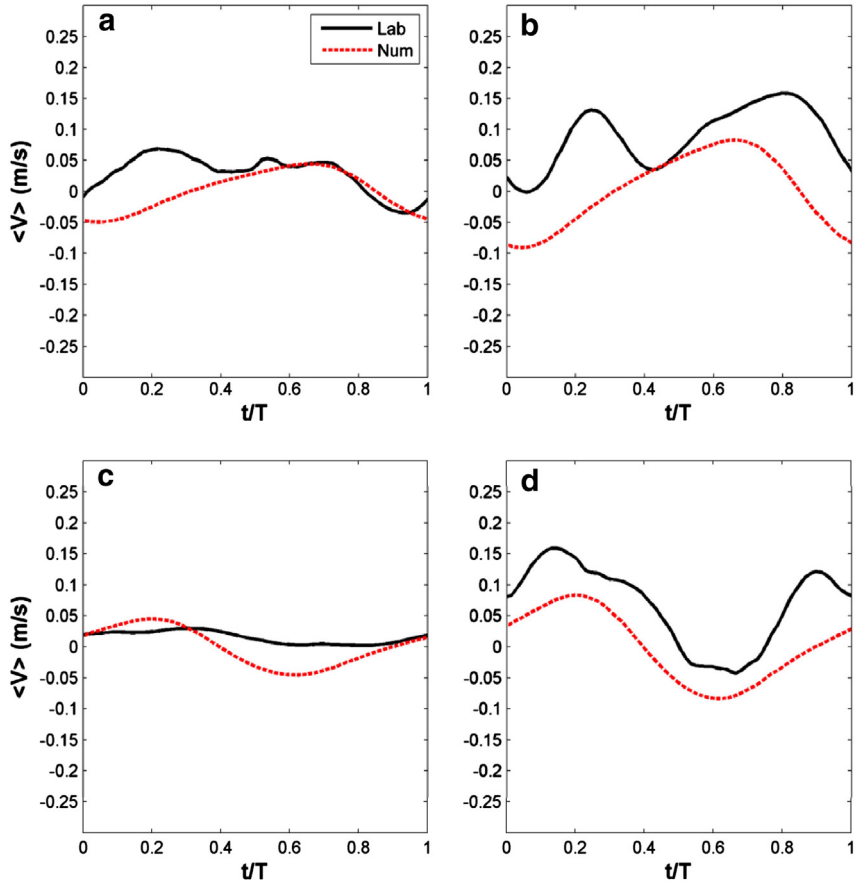

Fig. 15. Phase-averaged vertical velocities, <V>, inside the meadow for the experiment with N = 180 m^{-2}, h = 2.4 m, H = 0.5 m and T = 3.5 s. Experimental data (black solid line) vs numerical results (red dashed line). (For interpretation of the references to color in this figure legend, the reader is referred to the web version of this article.)

without swaying, are also displayed in order to evaluate how the calibration drag coefficient values fit to these formulations. The correlation coefficients found for both cases are high with values about 0.54 and relative errors smaller than 4%. Therefore, the calibrated drag coefficient values obtained for Asano et al. (1988) experiments fit to existing formulations.

Fig. 19 shows the obtained drag coefficients versus the associated Reynolds numbers for the Stratigaki et al. (2011) experiments. In this case Mendez et al. (1999) empirical relationships do not fit well to the obtained drag coefficient values. Although the formula for cases with movement fit well for Reynolds number between 4000 and 6000, large relative error and low correlation coefficient are found due to the discrepancies shown at low Reynolds numbers, range at which that formulation was not validated. Consequently, existing formulations are not appropriated for this case. This can be due to many different reasons: the larger experimental scale, the use of mimics with high flexibility and a range of Reynolds numbers have not been covered before. This points out the necessity of developing a new relationship for this type of cases where the flow conditions are different as well as the plant mechanical characteristics.

A new formulation is proposed looking for the best fit to the calibrated drag coefficient values. That formulation is shown in Fig. 19 and has the following expression:

$$C_D = 0.87 + \left(\frac{2200}{Re}\right)^{0.88} \tag{12}$$

Although a higher correlation coefficient and a smaller relative error than with Mendez et al. (1999) formulations are obtained, the values are still not good enough. Therefore, the drag coefficients achieved for Stratigaki et al. (2011) experiments do not fit to any existing formulation, neither to any formulation obtained using the based formula (11). For that reason, a new approach is needed in order to find the appropriate formulation for this case in which the vegetation is very flexible. The new approach, in which the vegetation movement is considered, is presented in the next section. Furthermore, the new approach allows estimating the relative velocity developed inside the meadow and with that the drag force exerted by the flow in the plants.

3.3. Analysis of coupling modeling of vegetation motion and flow

Looking for a better representation of the interaction between flow and vegetation the model for coupled movement described in Section 2 is considered. With this approach not only the drag force is considered but also the inertia, damping, restoring, gravitational, Froude–Krylov and hydrodynamic mass forces. Stratigaki et al. (2011) experiments are simulated with this new approach looking for better results. Only Stratigaki et al. (2011) experiments have been simulated using a coupled model because velocity measurements outside and inside the vegetation meadow are available. With this approach the plant swaying is solved and the velocity of this movement is used to calculate the relative velocity necessary in the drag force calculation. As a result, a new set of drag coefficients are obtained.

The vegetation motion equation depends on a set of coefficients that must be defined according to the mechanical model proposed in Eq. (4). The value of the added mass coefficient, C_m, is assumed to be equal to 1, as in Mendez et al. (1999) and Ikeda et al. (2001). The damping coefficient, C, depends on the mimic's properties, on its rigidity and its mass. The balance between these two coefficients will define the appropriate plant velocity. As the drag coefficient

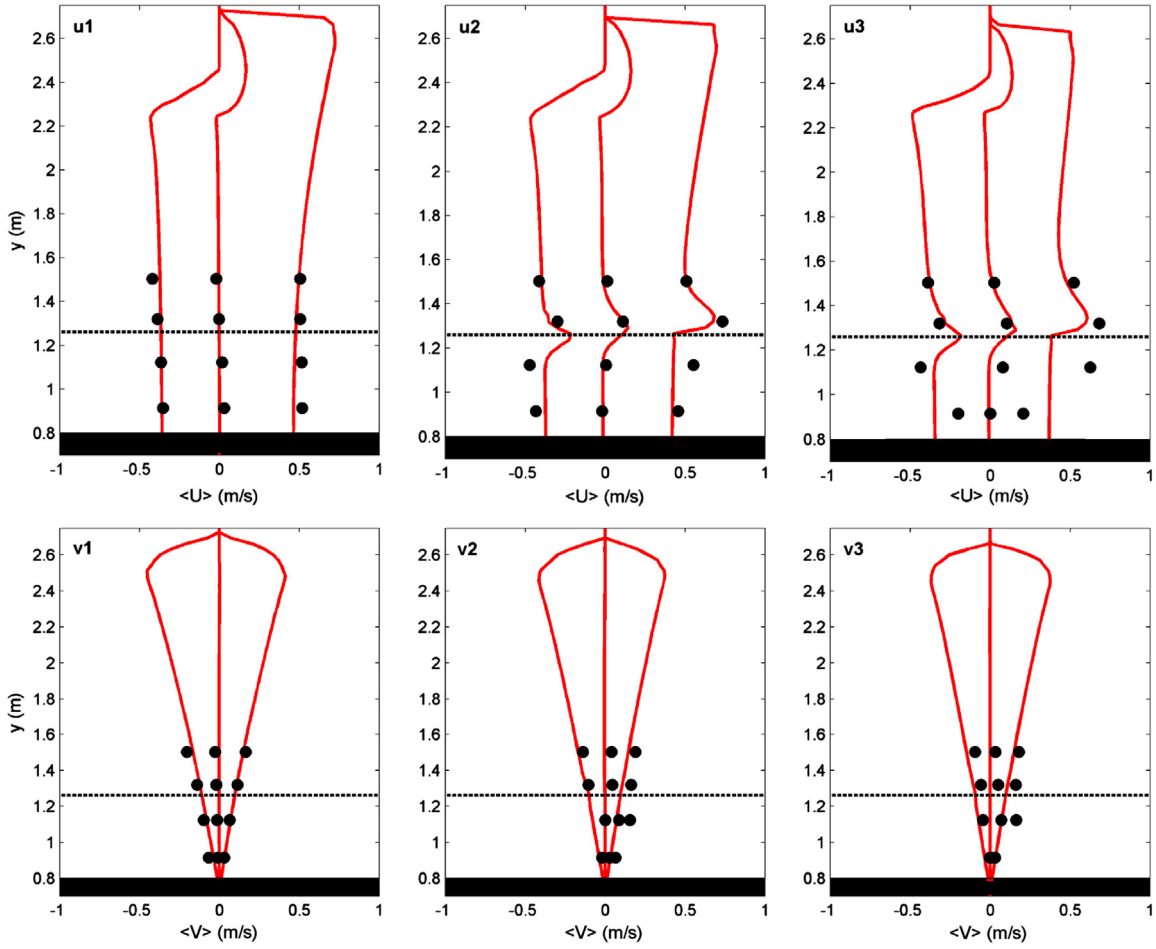

Fig. 16. Minimum, mean and maximum average horizontal (above) and vertical (below) velocity profiles at 0.7 m before the meadow, 2 m after its beginning and 2.7 m before its end. Experimental (black dots) and numerical results (red lines). The black dashed line represents the end of the meadow. Results for the experiment with N = 180 m^{-2}, h = 2.4 m, H = 0.5 m and T = 3.5s. (For interpretation of the references to color in this figure legend, the reader is referred to the web version of this article.)

depends on the flow properties, the damping coefficient depends on plant properties, which are constant, this second coefficient is set to a constant value. Therefore, the damping coefficient is set to simulate the swaying observed in the laboratory and the drag coefficient will be used as the calibration coefficient to match the energy attenuation in each one of the cases depending on flow characteristics. Unfortunately, plant movement was not directly measured in the experiments.

In order to determine the damping coefficient, a new set of laboratory experiments is carried at the University of Cantabria wave flume. It is 68.9 m long, 2 m wide and 2 m deep. The objective of this new set of experiment is to measure the magnitude of the plant bending under wave action. The upper plant excursion is used to calibrate the damping coefficient in Eq. (4).

The same mimics used in Stratigaki et al. (2011) are tested. Five mimics are inserted in a wood panel 2 cm thick attached to the flume floor and parallel to the flume sidewalls. The space between mimics is 5 cm, the same used by Stratigaki et al. (2011). The reason to use five mimics is to get plant–plant interaction during the plant bending, as it occurs in Stratigaki et al. (2011). Different regular wave conditions are considered. Wave period of 3, 4 and 5 s and wave height of 0.05, 0.10, 0.15 and 0.20 m are studied. The water depth is kept constant to 80 cm in all tests. The associated Reynolds number is between 1000 and 3500 for all the cases, in agreement with the range covered by Stratigaki et al. (2011).

Because the sidewalls of the flume are made of glass, plant motion can be measured by optical techniques. It is recorded by a 1 megapixel camera Marlin F131C of 8 bits of spectral resolution and with a frequency of 10 Hz. The camera is positioned perpendicular to the plane of plant movement. A calibration plate located at the plant plane is used to determine the correlation between pixels and meters. Synchronous measurements of free surface motion are made at the plant location and 4.65 m seaward this position, using a sampling frequency of 20 Hz. The synchronization of both measurements was done using a trigger at 10 Hz.

Fig. 20 presents an example of the maximum wave plant excursion for a regular wave case of H = 0.2 m and T = 4 s. The two upper panels represent the time history of the phase averaged free surface at the location of the plant. The lower pictures represent the maximum excursion onshore (left panel) and offshore (right panel). The corresponding wave phases when the maximum excursions are observed are represented using two dots in the free surface time series. The maximum excursion obtained for this case is of the order of 25–30 cm.

After sensitivity analysis made using wave excursion from the experiments and Eq. (4) a value of 12 Ns/m was chosen. This damping coefficient allows reproducing the plant movement amplitude and is in agreement with values found in the literature as the one proposed by Ikeda et al. (2001), 12.64 Ns/m for similar plant length and velocity regimes.

To calibrate the model, only the drag coefficient, C_d, in Eq. (4) is used to find the best fit to experimental data.

Fig. 21 shows the instantaneous positions of the plants under wave action at six different time steps every 0.5 s. The color scale represents the horizontal velocity magnitude while vegetation is represented by black lines. For a better visualization the plant motion is multiplied by a factor of 5 in the figure. As can be seen vegetation sways forced by the flow velocities. Positive horizontal velocity values,

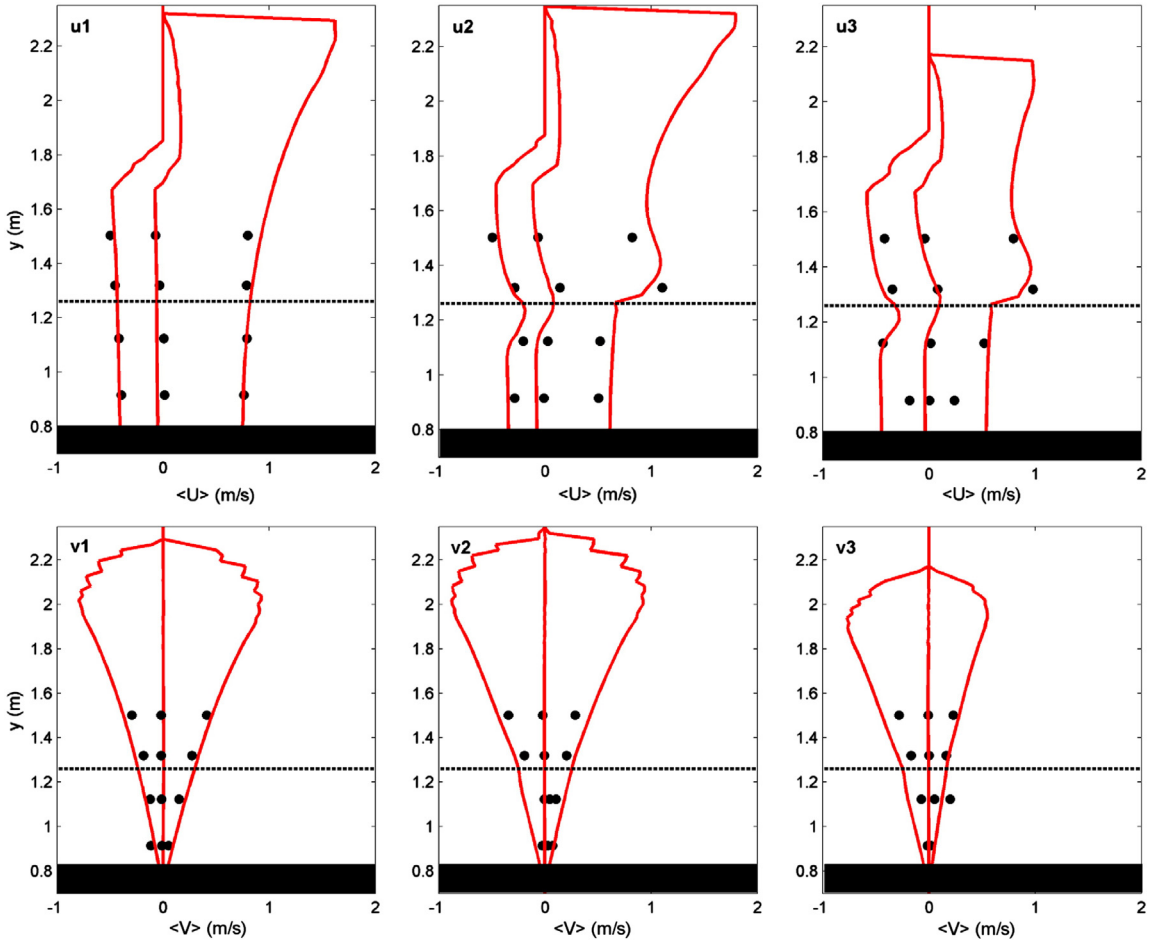

Fig. 17. Minimum, mean and maximum average horizontal (above) and vertical (below) velocity profiles at 0.7 m before the meadow, 2 m after its beginning and 2.7 m before its end. Experimental (black dots) and numerical results (red lines). The black dashed line represents the end of the meadow. Results for the experiment with N = 360 m^{-2}, h = 1.8 m, H = 0.5 m and T = 4 s. (For interpretation of the references to color in this figure legend, the reader is referred to the web version of this article.)

in red, produce a displacement of vegetation plants in the positive *x* direction. The same effect is found with negative velocity values, in blue, although the displacement is smaller due to the smaller magnitude of the velocity in that direction. This pattern is consistent with the one observed in the experiments indicating that the numerical model allows representing flow vegetation interaction. As can be seen, just above the vegetation field there is an increase in the velocity, skimming flow, due to the discontinuity in the momentum balance. This effect was also observed in the velocity profiles shown in Figs. 16 and 17.

Drag coefficients are set to obtain the best possible agreement between experimental and numerical wave height along the field. Numerical result for no swaying and swaying vegetation, is shown in Fig. 22 for one of the tests. As can be seen numerical results are almost identical but with different drag coefficients. In the case of swaying, the drag force introduced in the momentum equation is a function of the relative velocity developed between the plant and the flow. Taking into account this phenomenon the drag coefficient must be higher in order to obtain the same momentum reduction as in the case of no swaying vegetation and, consequently, the same wave attenuation along the vegetation field. The drag coefficient influence is shown in the same figure where two additional cases are displayed

Table 3
Coefficient proposed by Kobayashi et al. (1993) and Mendez et al. (1999) to relate drag coefficient with Reynolds number.

Author	α	β	γ
Kobayashi et al. (1993)	0.08	2.4	2200
Mendez et al. (1999) no swaying plants	0.08	2.2	2200
Mendez et al. (1999) swaying plants	0.40	2.9	4600

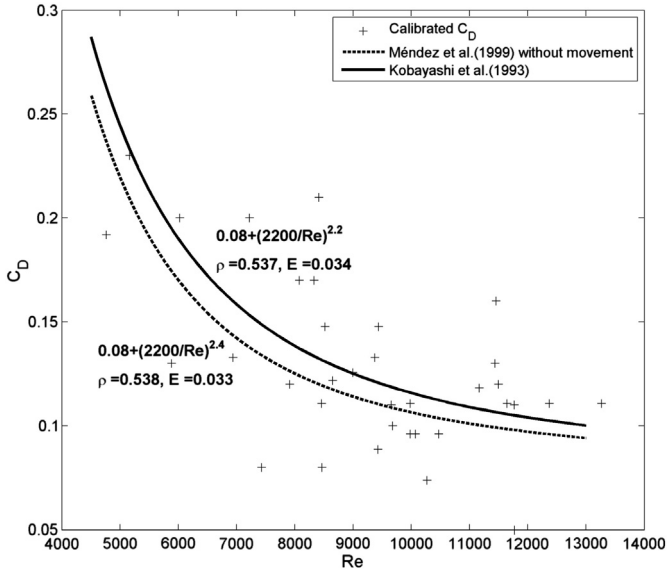

Fig. 18. Calibrated drag coefficient values for Asano et al. (1988) experiments. Kobayashi et al. (1993) and Mendez et al. (1999), without considering vegetation movement, empirical relationships are shown.

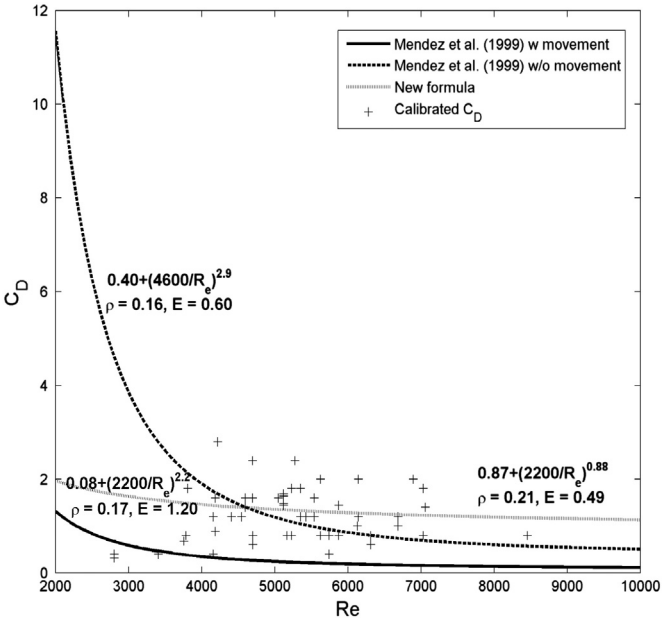

Fig. 19. Calibrated drag coefficient values for Stratigaki et al. (2011) experiments. Mendez et al. (1999), with and without considering vegetation movement, empirical relationships and a new adjustment (dotted line) are shown.

considering the drag coefficient for no swaying vegetation and a high drag coefficient. As can be observed, the drag coefficient which fits for no swaying vegetation is too small for the case in which the movement is considered and if this coefficient is too large the produced wave attenuation is also too high.

Wave velocities obtained with both approaches are also compared (Fig. 23) and, again, the results are almost identical. The maximum, mean and minimum velocity profiles along the vegetation field obtained considering swaying show the same velocity reduction inside the meadow and the same skimming flow obtained considering no swaying vegetation since the momentum reduction inside the vegetation is set to be almost equal with the increase of the drag coefficient.

Therefore, there are two approaches which can be used in order to obtain the wave attenuation produced by the meadow and the reduction in flow velocities. Both allow reproducing the problem taking into account the loss of energy produced by the vegetation meadow as a function of the drag coefficient but in the second case the physics involved in the coupled movement between the vegetation and the flow is considered. The drag coefficient is different for both approaches since the physics considered in each case is also different. Therefore, a different calibration of this coefficient is needed for the swaying approach. It can be concluded that in previous modeling efforts C_D fitting has taken care of interaction processes that have not been either properly modeled or even considered.

Following the same methodology used in the case of no swaying vegetation approach a new set of drag coefficients is obtained. These drag coefficients are represented in Fig. 24. The agreement of these new coefficients with existing formulas is evaluated by plotting them together with Mendez et al. (1999) formulations. Correlation coefficients and relative errors are calculated and displayed in the figure below the formulations. Although these estimators improve with this approach in comparison with the no swaying vegetation approximation for the formulation considering movement, the calculated relative error is very high. This disagreement is due to some different aspects. First, the experiments used to calibrate this coefficient are very different to the ones used by Mendez et al. (1999). The scale is larger and the vegetation is more flexible. Secondly, Mendez et al. (1999) swaying formulation was calibrated for Reynolds numbers between 2300 and 20,000 with a small amount of data in the low range. In this case, the range of Reynolds number varies mostly between 2000 and 7000 which means that the calibration is performed considering cases with less energetic wave conditions. Finally, the approach proposed by Mendez et al. (1999) to solve the problem of flow and vegetation interaction is based on a potential model whereas a model based on Navier–Stokes equations is proposed here, considering also the turbulent effects.

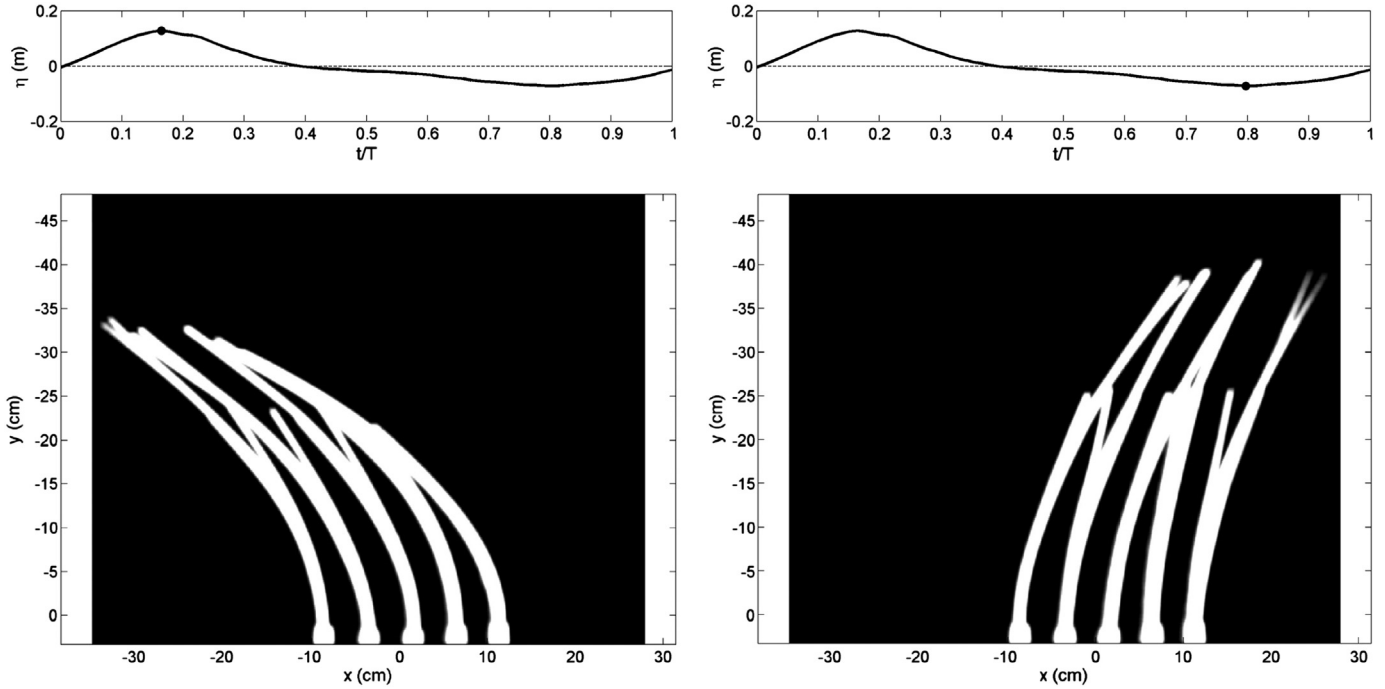

Fig. 20. Maximum wave plant excursion for a regular wave case of H = 0.2 m and T = 4 s. Upper panels: Time history of phase averaged free surface at the plant location. Lower left panel: maximum onshore excursion. Lower right panel: maximum offshore excursion. Dots represent the time where both maxima occurs in the wave phase.

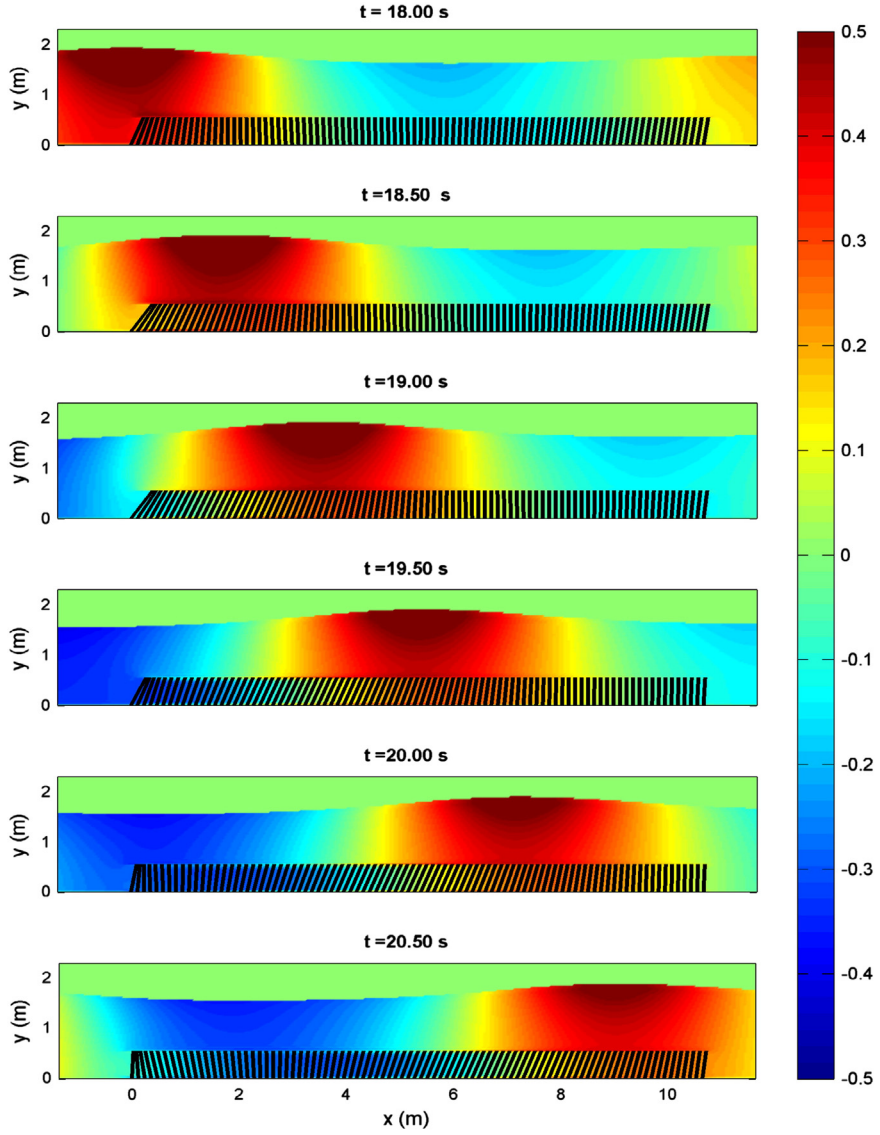

Fig. 21. Instantaneous vegetation field, black lines, position under wave action at six different times for the case with H = 0.5 m, T = 3.5 s, N = 180 strips/m^2 and h = 1.7 m over the meadow. Color scale represents the horizontal velocity magnitude. (For interpretation of the references to color in this figure legend, the reader is referred to the web version of this article.)

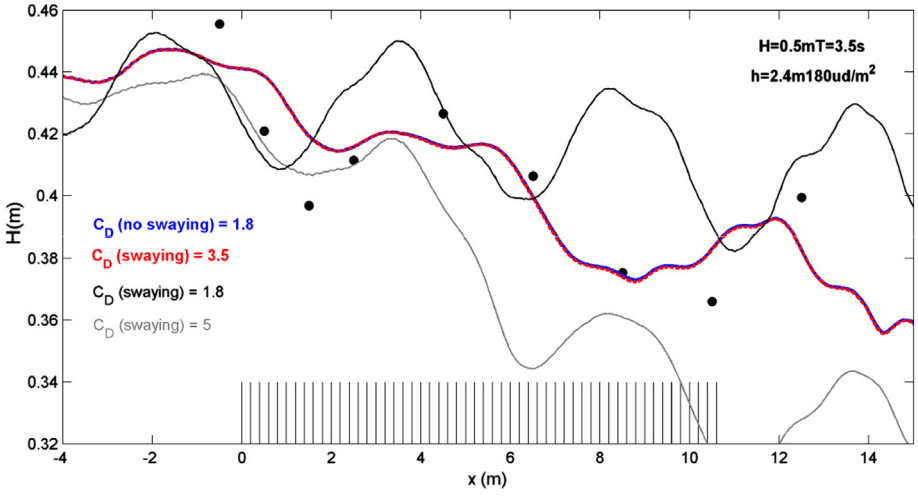

Fig. 22. Wave height evolution achieved considering no swaying vegetation (blue solid line) and flexible vegetation (red solid line) for a case with H = 0.5 m, T = 3.5 s, h = 2.4 m and N = 180 strips/m^2. Experimental measurements (black dots) and two additional cases for flexible vegetation with different C_D (solid black and gray line) are represented. (For interpretation of the references to color in this figure legend, the reader is referred to the web version of this article.)

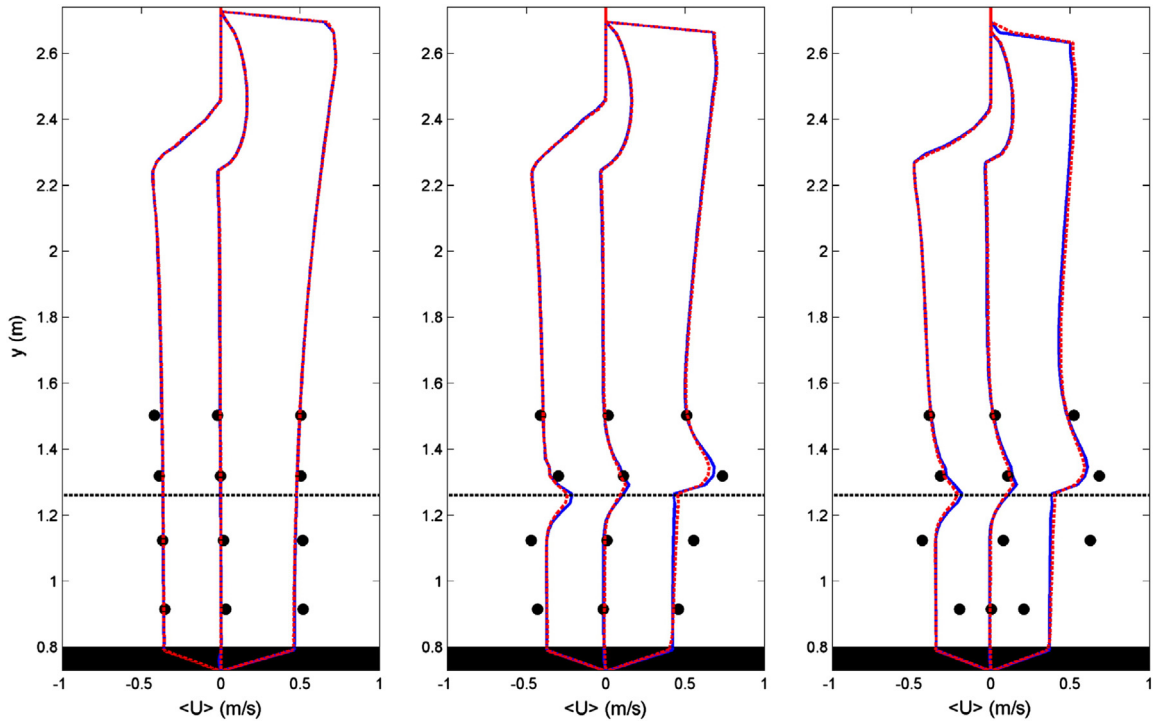

Fig. 23. Horizontal velocity profiles for no swaying (blue lines) and swaying (red lines) plants the case with H = 0.5 m, T = 3.5s, h = 2.4 m and N = 180 strips/m^2. (For interpretation of the references to color in this figure legend, the reader is referred to the web version of this article.)

Therefore, a new empirical relationship is proposed, based on the formulation given by Mendez et al. (1999) for cases with movement. This new relationship is as follows:

$$C_D = 1.61 + \left(\frac{4600}{Re}\right)^{1.9}. \quad (13)$$

This formulation provides a relative error smaller than those ones obtained using Mendez et al. (1999) formulations and a higher correlation coefficient. It gives a better estimation of the drag coefficient for cases with low values of the Reynolds number and in which the plant movement is considered.

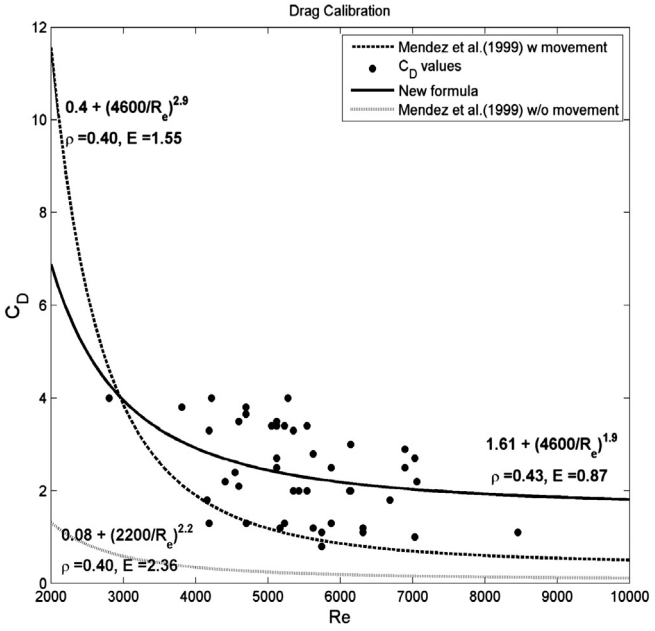

Fig. 24. Calibrated drag coefficient values for Stratigaki et al. (2011) experiments considering vegetation movement (black dots). Mendez et al. (1999) empirical relationships and a new formula (black solid line) are shown with the associated correlation coefficient, ρ, and relative error, E.

3.4. Analysis of drag force exerted by the flow on plants

A good estimation of the drag force produced by the flow on the plants can be used to study the vegetation survival or the possibility of having shoots torn off. As it has been demonstrated in previous sections, the modeling of the hydrodynamics processes produced by the plant on the fluid is very accurate considering vegetation with different mechanical properties. The difference lies on the value of the drag coefficient used to estimate the momentum damping exerted by the plants on the flow. However, when the effect of the fluid on the plant is calculated, flexible vegetation has to be considered in order to compute the wave plant excursion due to the waves since the velocity developed inside the meadow is the relative velocity between the flow and the plant motion and the drag force depends on this velocity.

Considering the coupled modeling the drag force is estimated as a function of the relative velocity. Therefore, the drag force exerted by the fluid on the plant is estimated more precisely with the presented model owing to including the plant motion. The drag force on the plant is estimated by vertically integrating the relative velocity determined by Eq. (5) using Eq. (1) to obtain the total force exerted over the plants. Figs. 25, 26, 27 and 28 display the drag force simulated numerically by the model. The force is presented in the plots per shoot and running meter.

Fig. 25 shows the influence of wave period in the drag force evolution along the vegetation meadow. Two cases with a vegetation density equals to 360 shoots/m^2, h = 2.2 m, H = 0.4 m and T = 3 and 4 s are considered. A direct relationship between the drag force and the wave period is observed obtaining larger values of the drag force with higher wave periods. A reduction in the drag force at the beginning of the meadow is observed, yielding a 35% reduction along the first 4 m and a gross damping of 55% at the rear end of the vegetation field.

The influence of wave height is also evaluated in Fig. 26 considering two cases with N = 360 shoots/m^2, h = 2 m, T = 3 s and H = 0.4

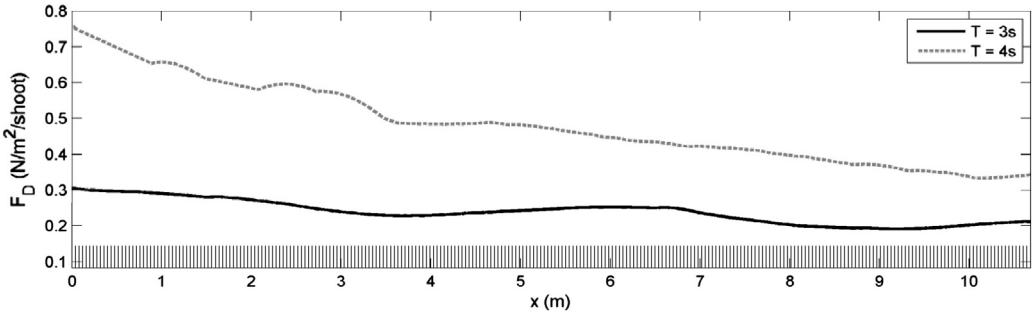

Fig. 25. Drag force evolution along the vegetation meadow for two cases with different wave periods: H = 0.4 m, h = 2.2 m, N = 360 m^{-2}, and T = 3 s, black solid line, and T = 4 s, gray dashed line.

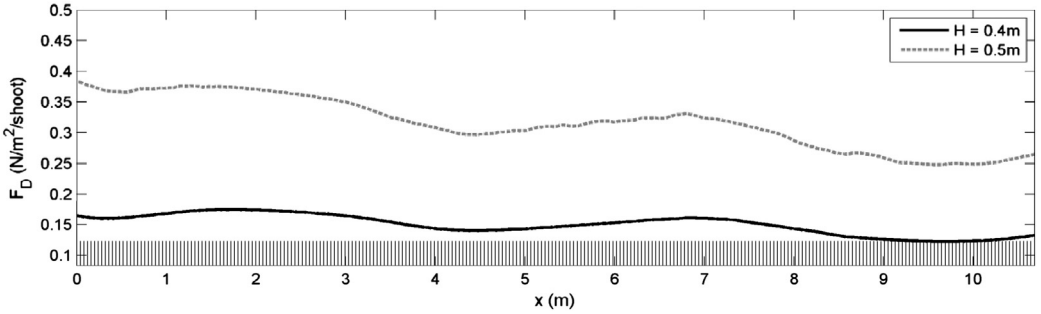

Fig. 26. Drag force evolution along the vegetation meadow for two cases with different wave heights: T = 3 s, h = 2 m, N = 360 m^{-2}, and H = 0.4 m, black solid line, and H = 0.5 m, gray dashed line.

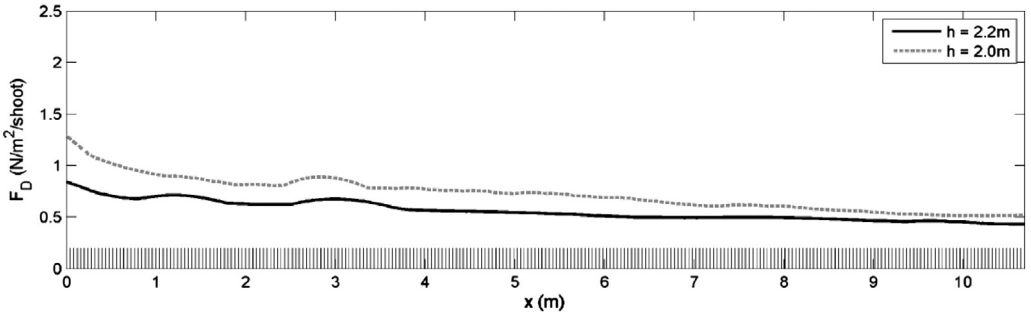

Fig. 27. Drag force evolution along the vegetation meadow for two cases with different water depths: H = 0.5 m, T = 3.5 s, N = 360 m^{-2}, and h = 2.2 m, black solid line, and h = 2 m, gray dashed line.

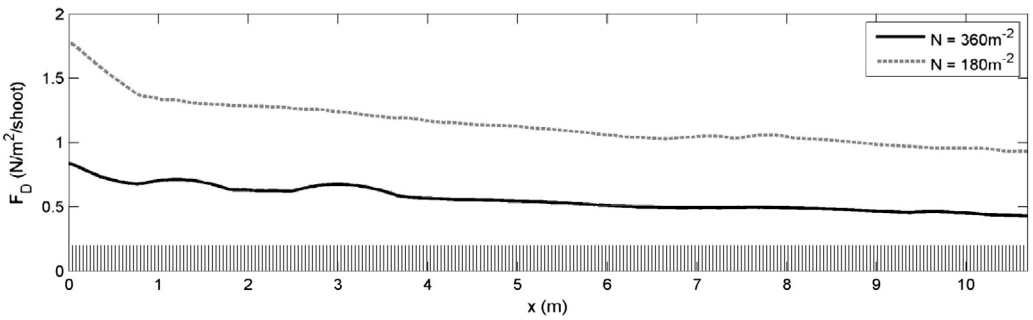

Fig. 28. Drag force evolution along the vegetation meadow for two cases with different vegetation densities: H = 0.5 m, T = 3.5 s, h = 2.2 m and N = 360 m^{-2}, black solid line, and N = 180 m^{-2}, gray dashed line.

and 0.5 m. Higher values of wave height induce larger drag forces in the field as expected.

The water depth influence is evaluated in Fig. 27. Two cases with H = 0.5 m, T = 3.5 s and N = 360 shoots/m^2 are compared considering two different water depths, h = 2.2 and 2 m. The increase in relative depth produces an increment of drag force on the plant due to the higher velocities of the fluid at the meadow since there is no breaking waves.

Finally, the influence of the vegetation density is studied. Fig. 28 shows the drag force evolution along the meadow for two different vegetation densities (180 and 360 shoots/m^2) under the same wave conditions (H = 0.5 m, T = 3.5 s and h = 2.2 m). The results show that the force on the individual shoots is higher for cases with lower plant density as expected.

4. Conclusions

In this paper the modeling of wave interaction with flexible swaying vegetation is addressed by solving numerically the RANS equations including the presence of the submerged plants in the model by a drag force and the turbulent flow by means of a k–ε model with closure equations incorporating the effect of vegetation in the flow. The fluid flow solution is coupled with a governing equation of the plant motion considering a linear deformation of the plant.

The new coupled model allows estimating the drag force exerted along the vegetation field as a function of the relative velocity between the fluid flow and the vegetation motion. The model ability to reproduce wave damping and the velocity field inside and outside the vegetation meadow is tested against different experimental setups, considering small and large-scale tests, swaying and no swaying plants.

Comparisons reveal a very good agreement between experimental and numerical results existing drag coefficient formulas for cases in which the vegetation swaying can be neglected. However, for flexible swaying plants it is shown that the best possible results can only be achieved by considering the coupling of the flow and the plant motion and by introducing a new drag coefficient formula which extends the range of Reynolds numbers previously explored.

In such a way, the new model provides very good comparisons with large-scale and flexible vegetation experiments for wave damping and velocity fields, inside and outside the meadow. Many of the limitations of existing models are overcome, opening the possibility to advance in the understanding of the two-dimensional interaction of real sea states with aquatic vegetation of diverse mechanical characteristics and geometries.

Acknowledgments

M. Maza is indebted to the MEC (Ministerio de Educación, Cultura y Deporte, Spain) for the funding provided in the FPU (Formación del ProfesoradoUniversitario) studentship (BOE-A-2012-6238). The support of the European Commission through FP7.2009-1, contract 244104 — Theseus ("Innovative Technologies for Safer European Coasts in a Changing Climate"), is also acknowledged.

References

Asano, T., Tsutsui, S., Sakai, T., 1988. Wave damping characteristics due to seaweed. Proc. of the 35th Coastal Eng. Conf. in Japan. Japan Soc. of Civil Eng, Matsuyama, pp. 138–142 (in Japanese).

Augustin, L.N., Irish, J.L., Lynett, P., 2009. Laboratory and numerical studies of wave damping by emergent and near emergent wetland vegetation. Coastal Engineering 56, 332–340.

Bouma, T.J., Temmerman, S., van Duren, L.A., Martini, E., Vandenbruwaene, W., Callaghan, D.P., Balke, T., Biermans, G., Klaassen, P.C., van Steeg, P., Dekker, F., van de Koppel, J., de Vries, M.B., Herman, P.M.J., 2013. Organism traits determine the strength of scale-dependent bio-geomorphic feedbacks: a flume study on three intertidal plant species. Geomorphology 180–181, 57–65.

Bradley, K., Houser, C., 2009. Relative velocity of seagrass blades: implications for wave attenuation in low-energy environments. Journal of Geophysical Research F: Earth Surface 114, F01004.

Bridges, K., Cox, D., Thomas, S., Shin, S., Rueben, M., 2011. Large-scale wave basin experiments on the influence of large obstacles on tsunami inundation forces. Proc. of the 6th International Conference on Coastal Structures, in Japan, pp. D1–D114.

Chen, S.N., Sanford, L.P., Koch, E.W., Shi, F., North, E.W., 2007. A nearshore model to investigate the effects of seagrass bed geometry on wave attenuation and suspended sediment transport. Estuaries and Coasts 30, 296–310.

Dalrymple, R.A., Kirby, J.T., Hwang, P.A., 1984. Wave diffraction due to areas of energy dissipation. Journal of Waterway, Port, Coastal, and Ocean Engineering 110, 67–79.

Dubi, A., Torum, A., 1995. Wave damping by kelp vegetation. Proc. of the 24th Coastal Eng. Conf. in New York. AM. Soc. of Civil Eng, pp. 142–156.

Dubi, A., Torum, A., 1997. Wave energy dissipation in kelp vegetation. Proc. of the 25th Coastal Eng. Conf in Orlando, 3, pp. 2626–2639.

DuPont, S., Gosselin, F., Py, C., de Langre, E., Hemon, P., Brunet, Y., 2010. Modelling waring crops using large-eddy simulation: comparison with experiments and a linear stability analysis. Journal of Fluid Mechanics 652, 5–44.

Elwany, M.H.S., O'Reilly, W.C., Guza, R.T., Flick, R.E., 1995. Effects of southern California kelp beds on waves. Journal of Waterway, Port, Coastal, and Ocean Engineering 121, 143–150.

Fonseca, M.S., Cahalan, J.A., 1992. A preliminary evaluation of wave attenuation by four species of seagrass. Estuarine, Coastal and Shelf Science 35, 565–576.

Gacia, E., Duarte, C.M., 2001. Sediment retention by a Mediterranean *Posidonia oceanica* meadow: the balance between deposition and resuspension. Estuarine, Coastal and Shelf Science 52, 505–514.

Guanche, R., Losada, I.J., Lara, J.L., 2009. Numerical modelling of coastal structures stability. Coastal Engineering 56 (5–6), 543–558.

Hiraoka, H., Ohashi, M., 2006. A (k–ε) turbulence closure model for plant canopy flows. Proc. of the 4th International Symposium on Computational Wind Eng. (CWE2006) in Yokohama.

Ikeda, S., Yamada, T., Toda, Y., 2001. Numerical study on turbulent flow and honami in and above flexible plant canopy. International Journal of Heat and Fluid Flow 22, 252–258.

Kobayashi, N., Raichle, A.W., Asano, T., 1993. Wave attenuation by vegetation. Journal of Waterway, Port, Coastal, and Ocean Engineering 119 (1), 30–48.

Koch, E., 2009. Non-linearity in ecosystem services: temporal and spatial variability in coastal protection. Frontiers in Ecology and the Environment 7 (1), 29–37.

Koftis, T., Prinos, P., Stratigaki, V., 2013. Wave damping over artificial *Posidonia oceanica* meadow: a large-scale experimental study. Coastal Engineering 73, 71–83.

Lara, J.L., Losada, I.J., Guanche, R., 2008. Wave interaction with low-mound breakwaters using a RANS model. Ocean Engineering 35, 1388–1400.

Lara, J.L., Ruju, A., Losada, I.J., 2011. Reynolds averaged Navier–Stokes modelling of long waves induced by a transient wave group on a beach. Proceedings of the Royal Society A 467, 1215–1242.

Li, C.W., Yan, K., 2007. Numerical Investigation of wave–current–vegetation interaction. Journal of Hydraulic Engineering 133, 7.

Losada, I.J., Lara, J.L., Guanche, R., Gonzalez-Ondina, J.M., 2008. Numerical analysis of wave overtopping of rubble mound breakwaters. Coastal Engineering 55 (1), 47–62.

Lowe, R.J., Koseff, J.R., Monismith, S.G., 2005. Oscillatory flow though submerged canopies: 1. Velocity structure. Journal of Geophysical Research 110, C10016.

Lowe, R.J., Falter, J.L., Koseff, J.R., Monismith, S.G., Atkinson, M.J., 2007. Spectral wave flow attenuation within submerged canopies: implications for wave energy dissipation. Journal of Geophysical Research C: Oceans 112, C05018.

Maza, M., 2012. Hydrodynamic study of *Posidonia oceanica* behaviour under oscillatory flow action. Master Thesis (in Spanish) Universidad de Cantabria.

Maza, M., Lara, J.L., Bouma, T.J., Ondiviela, B., Trinogga, J., Gordejuela, N., Losada, I.J., 2013. Experimental analysis of three dimensional wave and current interaction with real salt marshes. Internal Report (Theseus Project).

Mendez, F.J., Losada, I.J., 2004. An empirical model to estimate the propagation of random breaking and non-breaking waves over vegetation fields. Coastal Engineering 52, 103–118.

Mendez, F.J., Losada, I.J., Losada, M.A., 1999. Hydrodynamics induced by wind waves in a vegetation field. Journal of Geophysical Research 104, 18383–18396.

Nepf, H.M., Vivoni, E.R., 2000. Flow structure in depth-limited, vegetated flow. Journal of Geophysical Research 105 (C12), 28.547–28.557.

Ota, T., Kobayashi, N., Kirby, J.T., 2004. Wave and current interactions with vegetation. Proc. of 29th Coastal Eng. Conf. in Singapore, pp. 508–520.

Ruju, A., Lara, J.L., Losada, I.J., 2012. Radiation stress and low-frequency energy balance within the surf zone: a numerical approach. Coastal Engineering 68, 44–55.

Stratigaki, V., Manca, E., Prinos, P., Losada, I.J., Lara, J.L., Sclavo, M., Amos, C.L., Cáceres, I., Sánchez-Arcilla, A., 2011. Large-scale experiments on wave propagation over *Posidonia oceanica*. Journal of Hydraulic Research 49, 31–43.

Suzuki, T., Zijlema, M., Burger, B., Meijer, M.C., Narayan, S., 2011. Wave dissipation by vegetation with layer schematization in SWAN. Coastal Engineering 59, 64–71.

Terrados, J., Duarte, C.M., 2000. Experimental evidence of reduced particle resuspension within a seagrass (*Posidonia oceanica* L.) meadow. Journal of Experimental Marine Biology and Ecology 243, 45–53.

Torres-Freyermuth, A., Losada, I., Lara, J., 2007. Modeling of surf zone processes on a natural beach using Reynolds-averaged Navier–Stokes equations. Journal of Geophysical Research 112, L05601.

Torres-Freyermuth, A., Lara, J., Losada, I., 2009. Numerical modelling of short- and long-wave transformation on a barred beach. Coastal Engineering 57 (3), 317–330.